IMAGE: A MAP OF THE STARS OF THE ORION CONSTELLATION

Print ISSN: 2631-8490 Online ISSN: 2631-8504

JournalPreview

London Journal of Research in Science: Natural & Formal

Volume 25 | Issue 7 | Compilation 1.0

Great Britain Journals Press

WWW.JOURNALSPRESS.COM

Journal Content
In this Issue

Great Britain Journals Press

Hypothesis on the Etheric Spatial Structure of Electrons Exhibiting Wave-Particle Duality

Cheng Jinjun & Dian Cheng

Anhui University

ABSTRACT

Based on previous research, this paper proposes a revolutionary hypothesis about the essence of electrons. The study first draws on the innovative description of the wave-particle duality of photons in "Hypothesis on the Spatial Motion Mode of Photons", combines the theoretical derivation of the possibility of the existence of ether space in "Several Conjectures on the Existence of Ether", and the breakthrough idea of the electron structure model, and creatively puts forward the "Hypothesis on the Ether Space Structure of Electrons". This hypothesis challenges the traditional view in theories that regard electrons as point particles, and argues that electrons are essentially entities with a wave-particle duality/etherspace structure. This study systematically elaborates on the unique ether vortex structure and quantum dynamic behavior of electrons, constructs a brand-new theoretical framework to explainthewave-particle duality of electrons, and provides new understanding theoretical principles of basic particles such as electrons. This theoretical innovation not only helps to deepen the understanding of the essence of electrons, but may also open up new research-paths for unifying quantum mechanics and classical physics.

Keywords: electron; wave-particle duality; etheric space; structural model.

Classification: LCC Code: QC793.5.E425

Language: English

Great Britain Journals Press

LJP Copyright ID: 925671
Print ISSN: 2631-8490
Online ISSN: 2631-8504

London Journal of Research in Science: Natural & Formal

Volume 25 | Issue 7 | Compilation 1.0

Hypothesis on the Etheric Spatial Structure of Electrons Exhibiting Wave-Particle Duality

Cheng Jinjun[α] & Dian Cheng[σ]

ABSTRACT

Based on previous research, this paper proposes a revolutionary hypothesis about the essence of electrons. The study first draws on the innovative description of the wave-particle duality of photons in "Hypothesis on the Spatial Motion Mode of Photons", combines the theoretical derivation of the possibility of the existence of ether space in "Several Conjectures on the Existence of Ether", and the breakthrough idea of the electron structure model, and creatively puts forward the "Hypothesis on the Ether Space Structure of Electrons". This hypothesis challenges the traditional view in theories that regard electrons as point particles, and argues that electrons are essentially entities with a wave-particle duality/etherspace structure. This study systematically elaborates on the unique ether vortex structure and quantum dynamic behavior of electrons, constructs a brand-new theoretical framework to explainthewave-particle duality of electrons, and provides new understanding theoretical principles of basic particles such as electrons. This theoretical innovation not only helps to deepen the understanding of the essence of electrons, but may also open up new research-paths for unifying quantum mechanics and classical physics.

Keywords: electron; wave-particle duality; etheric space; structural model.

Author α: Bachelor of Economics graduate from Anhui University, China. Currently employed at Anhui Grain Engineering Vocational College. A hobbyist in physics and economics.
σ: MBA graduate from the University of Science and Technology of China. Currently employed at China Cinda Securities Anhui Branch. A hobbyist in economics and physics.

I. INTRODUCTION

In the development history of modern physics, the wave-particleduality of electrons has always been one of the most challenging core issues de Broglie proposed the hypothesis of matter waves, although quantum mechanics has successfully describedthewave-like and particle-like behaviors of electrons in mathematical form, there remains a fundamental confusion in explainingthephysical essence of this dual nature. The existing quantum theories are more phenomenological descriptions rather than essential explanations, which means that the understanding of the essence of electrons is still shrouded in a veil of mystery.

The author has made some breakthrough progress in previous research. In "Hypothesis on the Spatial Motion of Photons", an innovative three-dimensional helical model of photon motion was proposed, providing an intuitive physical picture for understanding the wave-particle duality of photons. In "Several ConjecturesConcerning the Existence of Ether", through rigorous logical reasoning and mathematical derivation, the possible status of the ether concept in modern physics was re-examined, and an electron structure model based on the ether space was initially constructed. These pioneering works have laid a solid theoretical foundation for the current in-depth research.

London Journal of Research in Science: Natural & Formal

Based on these previous achievements, this paper aims to propose a more complete and systematic theoretical framework- the"Hypothesis on the Etheric Spatial Structure of Electrons". Electrons are not point particles in the traditional sense, but rather an excited-state with an ether vortex space structure. Within this theoretical framework, the wave-particle duality of electrons can be naturally understood as two different manifestations inside and outside-the-the space structure of electrons: its particle nature corresponds to the self-integrity of the ether vortex space structure, while its wavenature reflects the frequency and wave properties of the circular motion of photon particles within the ether vortexspacestructure.This theoretical innovation has the following important scientific significance: First, it provides a physical explanation of the wave-particle duality of electrons based on the spatial structure; second, it establishes a connection between the quantum behavior of electrons and the microscopic structure of the ether space; third, it may provide new ideas for solving the fundamental problems of quantum mechanics; fourth, it builds a bridge between the quantum theory and the classical physical theory.

In the following chapters, we will elaborate on the theoretical basis, mathematical model of this hypothesis, as well as its ability to explain existing experimental phenomena in detail, and explore the possible theoretical breakthroughs it may bring.

II. ANALYSIS OF THE LIMITATIONS OF MAINSTREAMELECTRON STRUCTURE THEORIES

2.1 . The Evolution and Dilemmas of Classical Electron Models

2.1.1 Breakthroughs and Limitations of the Bohr Orbital Model

The Bohr model was the first to introduce quantum concepts into atomic structure, proposing the revolutionary idea that electrons move in specific orbits. This seemingly simple model successfully explained the regularity of the hydrogen atom spectrum, laying the foundation for quantum theory. However, upon closer examination, several fundamental problems with this model emerge. It cannot explain why electrons can remain stable in their orbits without radiating energy, nor can it account for the complex behavior ofmulti-electron atoms. Moreover, understanding the instantaneous nature of electron transitions remains a challenge. These unresolved mysteries suggest that there are significant gaps in our understanding of the nature of electrons.

2.1.2 Progress and Confusion of the Electron Cloud Model

The development of quantum mechanics led to the emergence of the electron cloud model, which replaced definite orbits with probability densities. This theory has been extremely successful mathematically, enabling precise predictions of the properties of various atoms and molecules. However, when we ask "what exactly is an electron?", the electron cloud only provides a vague probability distribution, unable to tell us the true state of an electron when it is not being observed. Although this probabilistic description is practical, it leaves profound philosophical and physical questions unanswered.

2.1.3 Achievements and Boundaries of the Energy Band Theory

In explaining the properties of solids, the energy band theoryhasdemonstrated its powerful capabilities. It depicts the collective behavior of electrons in crystals, successfully distinguishing between conductors, semiconductors, and insulators. However, this the is based on the assumption of an ideal periodic structure and often struggles with complex situations such as disordered systems and strongly correlated systems. More importantly, it still cannot answer the question of the fundamental properties of individual electrons.

2.2 Mysteries In Modern Electron Theories

2.2.1 Dilemmas of the Relativistic Description

Although the Dirac theory predicted the positron, the interpretation of negative energy states remains controversial. Although electron spin has been incorporated into the theoretical framework, its physical origin remains unclear. These deep-seated problems indicate that even in the most advanced relativistic quantum theories, our understanding of electrons is still incomplete.

2.2.2 Electrons in the Standard Model

In the Standard Model of particle physics, electrons are treated as point particles with no internal structure. Quantum electrodynamics, the quantum theory describing electromagnetic interactions, views electrons as points with no spatial extent and can calculatetheinteractions between electrons and electromagnetic fields with extremely high precision. These calculation results are highly consistent with high-precision experimental data. So far, in high-energy physics experiments, even at extremely high-energy scales, electrons still behave like point particles without discernible internal components. However, some cutting-edge theories and research suggest that although the view of electrons as point particles is simple, it brings infinite mathematical difficulties and avoids the fundamental origin of electron mass and charge. In some higher-precision electron-electron scattering experiments, when the energy is extremely high, there are small deviations within the error range in the experimental data. Some physicists speculate that this may be due to the internal structure of electrons having an extremely small scale (non-point particles). Although there is currently not enough evidence to overturn the mainstream view that electrons are point particles, these experiments continue to challenge the limits of the concept of electrons as point particles, indirectly reflecting the significance of the hypothesis that "electrons have a radius"intheoretical exploration. The interaction mechanismbetweenelectrons and other particles remains a mystery at a deeper level.

2.3 Common Limitations of Existing

Theories All current electron theories face several fundamental challenges. Firstly, there is a lack of a physical picture of wave-particle duality. We lack a model that can intuitively show how electrons simultaneously possess both wave-like and particle-like characteristics. Secondly, there is a disconnect between quantum and classical descriptions. It is unclear how the determinism of the macroscopic world emerges from quantum probability. Thirdly, there is confusion about the nature of the measurement process. There is no consensus on how observation affects the state of an electron. Fourthly, there is a void in the description of spatial structure. Existing theories avoid the question of whether electrons may have an internal structure. These deep-seated problems are not technical but conceptual. They suggest that we need a newperspectivetounderstand the nature of electrons. This understanding may require breaking away from the traditional concept of "point particles" and viewing electrons as entities with more complex spatial structures. This is precisely the starting point for the Etheric Spatial StructureHypothesis that we will explore next.

III. INCOMPLETENESS OF THEORETICAL FORMULAS RELATED TO ELECTRONSTRUCTURE

3.1 In-depth Analysis of the Deep Problems of the de Broglie Wave length Formula

The de Broglie wavelength formula（λ =h/p, as one of the cornerstones of quantum mechanics, has successfully established a mathematical connection between particle-like and wave-like properties. However, it still has several key deficiencies in terms of physical essence.

3.1.1 Uncertainty of the Kinematic Mechanism

This formula directly associates the wavelength with momentum but fails to clarify the underlying physical mechanism. For an electron with rest mass, its spatial motion velocity is always lower than the speed of light, which is fundamentally different from the motion characteristics of photons. An important question is, as a non-relativistic particle, from which physical process does the wave-like property of an electron originate? The formula itself does not provide a dynamic explanation but merely establishes an empirical mathematical relationship.

3.1.2 Implicit Requirements for Spatial Structure

The application of the formula actually implies that an electron cannot be a mathematical point particle. If an electron indeed exhibits wave-like properties, and a moving electron cannot move in a helical straight line in space like a photon to generate a wavelength and frequency, then it must have some kind of spatial extension structure. What is the relationship between this structure and the wave length? Is it a whole-body vibration or a partial excitation?Existing theories remain silent on these key issues, leaving the physical essence of the de Broglie wavelength still ambiguous.

3.1.3 Lack of Unified Description of Wave-Particle Duality

Although the formula formally connects particle-like and wave-like properties, it fails to provide a unified physical picture. It neither explains how an electron "carries" wave-like properties nor how the wave-like property "collapses" into particle-like property during observation. This disconnect between form and essence reflects the incompleteness of the theory at the fundamental level.

3.1.4 Limitations in Dealing with Relativistic Effects

When the velocity of an electron approaches the speed of light, the change in its mass will significantly affect the wavelength calculation. Although the formula can be improved by introducing the relativistic correction factor γ , this correction is external and fails to fundamentally solve the limitations of the theoretical framework. In addition, when the electron is at rest ($v = 0$), the formula predicts that the wavelength is infinite, which is obviously inconsistent with actual observations. This anomaly suggests that it may be necessary to re-examine the concept of "rest" itself or consider the inherent internal motion characteristics of the electron. All these incompletenesses are not only related to the degree of perfection of a specific formula but also touch on the fundamental conceptual framework of quantum theory. To break throughtheselimitations, it may be necessary to develop a brand-new theoretical paradigm that takes into account the internal structure, spatial properties, and quantum behavior of electrons in a unified manner.

3.2. In-depth Discussion on the Compton Wavelength Formula.

The phenomenon associated with the Compton wavelength originates from the elastic scattering process between photons and stationary electrons. The Compton wavelength formula is: $\lambda = h/(m_0 c)$. Where h is Planck's constant, reflecting the quantization characteristics of energy in the microscopic world; m_0 is the rest mass of the electron, describing the intrinsic property of the electron in a stationary state; c is the speed of light in a vacuum, playing a central role in relativity and electromagnetism. This formula succinctly reveals the key laws of the interaction between photons and electrons in the microscopic world. It not only has significant descriptive value in the electron system but also shows a certain degree of universality when its theory is extended to other particles(such as protons, neutrons, etc.). The Compton wavelengths of different particles are inversely proportional to their respective masses.

The Compton wavelength formula is based on several key idealized assumptions: first, the electron is abstracted as a point particle with no size; second, the interaction is assumedtobecompleted instantaneously; third, only electromagnetic interactions are considered. Although the idealized Compton wavelength formula has achieved remarkable success in explaining basic physical phenomena such as the Compton effect, it is far from perfect and has obvious limitations.

First of all, the assumption regarding the electron as a point particle may no longer be applicable in some extreme cases. With the development of high-energy physics experimental techniques, research on the internal structure of microscopic particles has become increasingly in-depth. In fact, modern physics believes that electrons may have some kind of internal structure or a certain degree of spatial extensibility. Under this new understanding, the assumption of a point particle may be overly simplified and unable to accurately describe the real behavior of electrons during the scattering process with photons. For example, the internal structure of an electron may cause changes in the energy and momentum distribution during the scattering process, thereby affecting the measurement results of the Compton wavelength.

Secondly, the assumption that the interaction is completed instantaneously is also too idealistic. In the real world, interactions in the microscopic world are often a complex and time-consuming process, involving the coupling and evolution of multiple quantum fields. The assumption of instantaneous interaction ignores the temporal characteristics of the interaction, which may lead to deviations when describing some complex scattering processes. Finally, the limitation of only considering electromagnetic interaction is gradually emerging. The interaction of microscopic particles is a complex many-body system. In additiontoelectromagnetic interaction, there are other fundamental interactionssuch as weak interaction and gravitational interaction. Although in the photon-electron scattering process, the contributionofelectromagnetic interaction usually dominates, in some specificcases, other weak interactions may also have a non-negligible impact on the scattering results.

In conclusion, although the Compton wavelength formula is of great value in describing and explaining some basic physical phenomena, it is only an approximate theory established based on specific idealized assumptions. The Compton wavelength formula may be a special case in a more fundamental and complete theoretical system. It awaits further development and improvement based on new theoretical and experimental research tomorrow comprehensively and accurately revealing the physical essence of the microscopic world.

3.3. In-depth Discussion on the Schwarzschild Radius Formula

The Schwarzschild radius formula describes how small an object with a given mass needs to be compressed in order to become black hole. The formula is $Rs=2GM/c^2$, where Rs is the Schwarzschild radius, G is the gravitational constant, Mis the mass of the object, and c is the speed of light in a vacuum. The derivation of the Schwarzschild radius formula is as follows:

Suppose an object of mass m is emitted from the surface of a celestial body with mass M, and the radius of the celestial body isR. At the moment of emission, the object has kinetic energy$E_K=(1/2)mv^2$. At the same time, since the object is in the gravitational field of the celestial body, it has gravitational potential energy $E_P=-GMm/R$ (here, the gravitational potential energy at infinity is defined as 0, so the gravitational potential energy on the surface of the celestial body is negative). At this time, the total mechanical energy of the object is $E_1=E_K+E_P=(1/2)mv^2-GMm/R$. When the object escapes to infinity, it can be considered that the object is no longer affected by the gravitational force of the celestial body, so the gravitational potential energy $E'_P=0$; if the object can just escape, then its velocity is exactly 0 when it reaches infinity, that is, the kinetic energy $E'_K=0$. Therefore, the total mechanical energy of the object at infinity is $E_2=E'_K+E'_P=0$. Since only gravity does work during the motion of the object,

mechanical energy is conserved, that is, $E_1=E_2$. Then $(1/2)mv^2-GMm/R=0$. By rearranging and solving for v, we can obtain the escape velocity formula $v=\sqrt{2GM/R}$. Therefore, $R=2GM/v^2$.

Based on this escape velocity formula, Schwarzschild inferred that when R is continuously compressed until the mass produces a black hole effect, even light cannot escape. Therefore, v =c, and the is obtained. Schwarzschild radius formula Rs=2GM/c

However, what I would like to point out here is that theSchwarzschild radius formula is derived based on general relativityand does not take into account the effects of quantum mechanics. When the escaping matter is a photon, it is inappropriate to directly transform the formula $(1/2)mv^2-GMm/R=0$ into $(1/2)mc^2-GMm/R=0$. This is because the velocity of the escaping photon is c. As a relativistic particle with zero rest mass, the kinetic energy of a photon exhibits characteristics that are completely different from those of classical particles. According to Einstein's mass-energy relation, the total energy E of a photon has a simple and direct relationship with its momentum p: E = pc. The energy of a moving photon is mc^2, and it is all manifested as kinetic energy, rather than $(1/2)mc^2$. Therefore, the photon escape formula should be^2 - GMm/R = 0, and accordingly, the Schwarzschild corrected to mc radius formula should be corrected to $Rs=GM/c^2$.

3.4. In-depth Discussion on the Planck Mass

The Planck mass formula $M_P=\sqrt{\hbar c/G}$ (the specific formula i missing here, but we'll keep the structure for translation) marks the mass scale at which the effects of quantum mechanics and general relativity are both significant. As a fundamental physical constant, the Planck mass has important physical significance. However, the reare significant limitations in its derivation process: this mass scale is purely obtained through the dimensional analysis combination of three basic constants (reduced Planck constant ħ, speed of light c, and gravitational constant G). Although this construction is methodismathematically concise, it lacks a profound physical mechanism explanation. That is, it does not clarify why the combination of these three specific constants has a mass meaning; it fails to explain how quantum effects (ħ) and gravity (G) are specifically coupled; the introduction of the speed of light c only ensures the dimensional correctness and does not reflect the internal connection between relativity and quantum mechanics.

Quantum theory indicates that when the Compton wavelengths equal to the Schwarzschild radius, the obtained mass is the Planckmass $M_P=\sqrt{\hbar c/G}$ (the specific formula is missing here). The Planckmass is also the minimum possible black hole mass. If the mass of a black hole approaches the Planck mass, its Schwarzschild radius approximately the Planck length $L_P=\sqrt{\hbar G/c^3}$ (the specific formulais missing here).

We will attempt to derive it based on this. The Compton wavelength formula is $\lambda=h/(m_oc)$, where h is the Planck constant, mo is the particle mass, and c is the speed of light in a vacuum. The Schwarzschild radius formula is $Rs=2GM/c^2$, where G is the gravitational constant and M is the mass of the celestial body. When the Compton wavelength is equal to the Schwarzschild radius, that is, $\lambda=Rs$. Substituting the above two formulas, we get: $m=\sqrt{\hbar c/2G}$. Since both m_o and M on both sides of the equation represent mass, we can unify them with m. Then, by rearranging and solving the equation, we get $m=\hbar c/2G$ (the specific result is missing here). However, this result has a relatively large deviation from the Planck mass $M_P=\sqrt{\hbar c/G}$ formula is missing here). Nevertheless, the physics community believes that the Planck mass presented in this way is consistent in terms of order of magnitude and physical meaning. Essentially, it is a characteristic mass defined by combining the basic constants of quantum mechanics and general relativity within the framework of quantum gravity.

Based on a systematic analysis of existing electron theoretical models and their related formulas, we have found that these theories all have problems of insufficient explanatory power and internal

contradictions to varying degrees. These theoretical difficulties are mainly reflected in the following aspects:

At the theoretical description level, whether it is Bohr's quantized orbit model, Schrödinger's electron cloud model, or Dirac's relativistic electron theory, none of them can fundamentally clarify the physical essence of the wave-particle duality of electrons. Although these theories have achieved success in mathematical form, they leave many unsolved mysteries in the physical picture.

Secondly, at the formula application level, important relationships such as the de Broglie wavelength formula and the Compton wavelength formula are all based on the idealized assumptionofregarding the electron as a point particle. Although this simplified treatment is effective within a certain range, it cannot explain the possible internal structural characteristics of the electron, nor can it fully describe the complex process of the interaction between the electron and the electromagnetic field.

Thirdly, at the experimental observation level, with the continuous improvement of measurement accuracy, the discovery of some fine-effects (such as the anomalous magnetic moment of the electron)poses a severe challenge to the traditional point-particle electrode. These experimental results suggest that the electron may have a more complex spatial structure and dynamic characteristics.

In view of the above theoretical difficulties, we attempt to break free from the constraints of traditional theories and construct a brand-new electron model with a spatial structure.

IV. REVIEW OF RELATED PREVIOUS WORK

4.1. Description of the Wave-Particle Duality of Photons

In *Hypothesis on the Spatial Motion Mode of Photons* the author comprehensively, deeply, and intuitively describes the wave-particle duality of photons through a specifically constructed physical model and rigorous mathematical analysis methods. The wave-particle duality of photons is one of the most fascinating phenomena in the microscopic world.

The author points out that the wave-particle duality of photons is not simply a superposition of two properties but achieves a high degree of organic unity in its spatial motion process. The actual motion trajectory of a photon exhibits a uniformly constant helical linear motion. This unique motion mode is a perfect combinationofuniform circular motion and uniform linear motion perpendicular to the plane of the circle. From the perspective of spatial motion, the propagation of photons in the ether space is not a simple linear or curvilinear motion but a helical motion that incorporates complex geometric shapes and dynamic characteristics.

This motion mode enables photons to exhibit both the discrete characteristics of particles and the continuous characteristics of waves under different conditions, thus truly achieving the unityofwave-particle duality. Therefore, the particle energy formula of is directly equivalent to the wave energy formula of photons $E = mc^2$ photons $E = hv$, that is, $E=mc^2= hv$.

4.2. Description of the Wave-Particle Duality of Electrons

In the research *Several Hypotheses about the Existence of Ether*, starting from the contradictory phenomena in multiple classical physical experiments and modern physical theories, the author deduces the physical possibility of the existence of ether space through rigorous logical reasoning and theoretical construction. The paper puts forward a novel and bold hypothesis: ether is not only the carrier of negative energy and the stream of consciousness but also a component of space itself. In traditional physical concepts, space is regarded as an absolute, unstructured background. However, in

this hypothesis, ether endows space with new connotations and attributes. Ether constructs all things in the universe by capturing photons and transforming them into fundamental particles. This construction process is not accomplished overnight but a complexand orderly one.

Regarding the particle structure model, an innovative view is further proposed. That is, fundamental particles such as electrons, protons, and neutrons are formed by the combination of photons and ether spheres. Specifically, photons move in a uniformly accelerated helical linear motion in the ether space. When a photon encounters a dense ether space, its linear motion changes and transforms into circular motion. This change in motion is not simply a change in direction but is accompanied by a strong interaction between the photon and the ether. During this process, the photon captures part of the ether to form an ether sphere. The point photon then moves in an S-shaped closed loop around the surface of the ether sphere. Through this complex motion mode, fundamental particles such as electrons are ultimately formed.

This brand-new particle structure model provides a deeper and more comprehensive perspective for us to understand the origin and essence of fundamental particles. It not only helps to explain some classical mechanical phenomena that have long puzzled physicists and cannot be explained by classical mechanics, such as electronspin and perturbation problems in quantum electrodynamics, but also provides a new theoretical basis and research direction for us to explore the microscopic structure and evolutionary history of the universe. This model is expected to become a bridge connecting the microscopic and macroscopic, classical and modern physics, promoting the innovation and development of physical theories.

V. THE CONCEIVED ELECTRON ETHER SPACE STRUCTURE MODEL

Based on the existence of the ether space, we have conceived the formation process of electrons. An electron is regarded as being formed by a point photon moving in an S-shaped closed loop around the surface of an ether sphere. The linear velocity of this point photon moving in an S-shaped loop around the surface of the ether-sphere is 2c (c is the speed of light in a vacuum). Meanwhile, the ether sphere itself also undergoes self-rotation and other motions. This series of conceptions lays the foundation for further research on the connection between the wave-particle duality of electrons and the ether space.

5.1 The ether space is the absolute space

In *Several Hypotheses about the Existence of Ether*, it is proposed that the ether space is a medium with complex structures and dynamics. Electrons exist in the ether space, and their various properties are closely related to the characteristics of the ether space. The self-rotation of the ether sphere and the motion of the point photon on its surface together constitute the basis for the motion of electrons in the ether space.

In our hypothesis, we propose that the ether is the space itself, and there is no void. Therefore, the speed c of light in a vacuum is the speed of light in the ether space. From this, it can be seen that the speed of light is relative to the ether space coordinate system. Since the speed of light c is constant, the ether space coordinate system relative to the constant speed of light must be absolutely stationary. The absolute space should refer to a space whose spacetime coordinate system has absoluteness. An object that is stationary relative to this coordinate system is absolutely stationary; an object that is moving relative to this coordinate system is in absolute motion. However, the absolute space itself can expand and undergo bending deformation. If it is found that after a certain fundamental particle in the ether space is collided by a photon, the photon does not produce a Doppler effect (that is, the frequency and wavelength of the photon do not change after being bounced back by the collision), then it can be said that this fundamental particle is absolutely stationary in the ether space.

For a stationary electron, its photon particles maintain an S-shaped closed-loop rotational motion along the surface of the ethersphere, and the ether sphere also maintains self-rotation at the same time. However, the ether sphere space coordinates of the electron can remain stationary relative to the ether space coordinate system. Therefore, the electron has a rest mass. Photons are always moving in the ether space and cannot be stationary relative to the ether spacecoordinate system. Therefore, photons have no rest mass but only motion mass.

5.2. The Ether Space Structure Model of Electrons

Based on the above hypothesis and combined with electron theory and relevant properties, we conceive a model of an electron that is absolutely stationary in the ether space. This electron-has-wave-particle duality ether space structure, specifically as follows: A photon with a motion mass of m is captured by the dense ether and fuses into an ether sphere (with a sphere radius of r) to form an electron. The photon particle moves in an S-shaped closed-loop around the surface of the ether sphere. The essence of the S-shaped circular motion of the photon particle is a combined motion of two circular motions in mutually perpendicular planes. The linear velocity of the photon particle along the directions of the two circular planes is both c, and the linear velocity of the composite motion of the photon particle is 2 c. The photon in the electronether sphere has positive energy, while the ether sphere has negative energy. Due to the capture of the helically moving photonandtheinfluence of the circular motion of the photon, the ether sphererotates continuously like the Earth. For a point on the equatorial plane of the ether sphere shell (similar to the position of the Earth's equator), which is perpendicular to the axis of rotation and at a distance of r from the center of the sphere, its linear velocity of motion is also c. For an electron that is absolutely stationaryintheether space, its rest mass is the motion mass of the photon particle moving around the ether sphere. The energy of a stationary electron satisfies both the relativistic and quantum energy formulas: $Ee = mc^2 = hv$. The positive energy of the photon moving around the surface of the ether space in the electron and the negative energy of the ethersphere always remain equal; when the positive energy of the photon in the electron ether sphere changes, the negative energy of the ether-sphere also changes simultaneously. The larger the motion frequency of the photon particle in the electron ether sphere, the greater the rest mass of the electron, the shorter the wavelength, the smaller the volume of the ether sphere, and the higher the negative energy density of the ether sphere; conversely, the smaller the rest mass of the electron, the longer the wavelength, the larger the volume of the electron ether sphere, and the lower the negative energy density of the sphere (Figure 1).

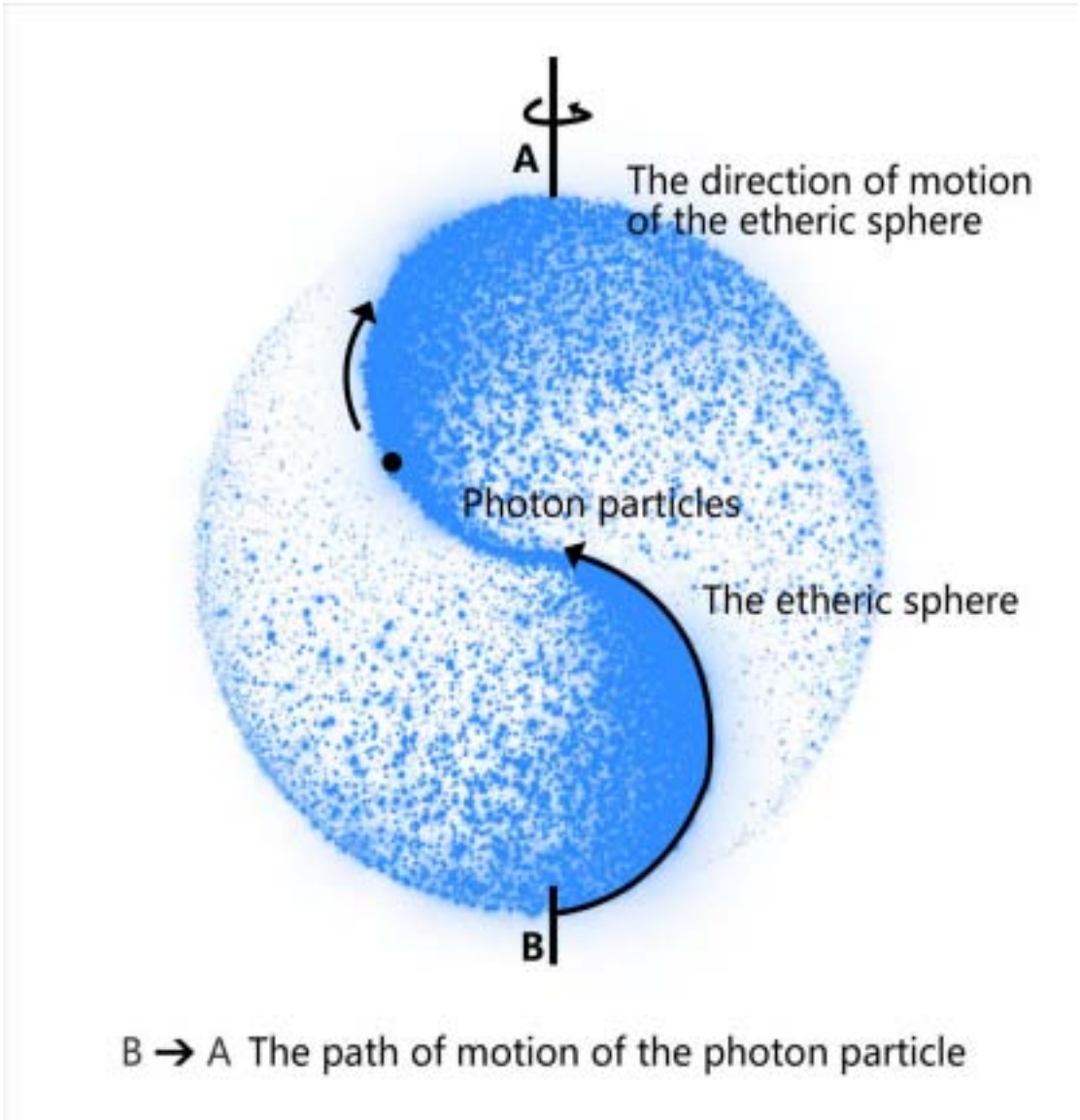

Figure 1: Is a model of a fundamental particle, the electron. B→A is the trajectory of a photon particle moving along the surface of another sphere, which is a closed S-shaped curve. The linear velocity of the photon particle moving on the surface of the ether sphere is 2c. The ether sphere rotates around its axis of rotation. The radius of the electron is r, the wavelength of the electron is 2πr, the frequency of the electron is c/（2πr, and the rest mass of the electron is m.

5.3 Characteristics of the Ether Sphere

The author's previous research has pointed out that ether vortices from ether spheres through continuous self-rotation, creating a boundary between fundamental particles and the ether space and giving rise to the self-category of fundamental particles. The ether sphere of an electron coincides with the cosmic ether space. As we know, the cosmic ether space is a continuous whole, in which the dense ether space is formed by the superposition of ether negative energy. Therefore, the ether spheres that make up fundamental particles such as electrons are completely coincident with the cosmicether space in terms of extension. The ether sphere of an electron is formed by the capture of ether from the dense ether space by photons. The ether sphere of an electron coincides completely with the cosmic ether space, and the self-rotation of the ether sphere does not drive the rotation of the corresponding ether space.

5. 4. Interaction between the Ether Sphere and the Electron

Within the proposed theoretical framework of the electron ether space, through qualitative analysis of the properties of the ethersphere and its interaction with the electron, we have established a correspondence between the properties of the electron and the characteristics of the medium. The ether sphere is described as a dynamic medium with specific physical properties. In such a medium environment, the physical properties of the electron are deeply associated with the characteristics of the ether sphere:

5.1 Basic Properties of the Ether Sphere: It serves as the physical background that carries electromagnetic phenomena and quantum effects; it has elastic restoring force and energy storage capacity; it exhibits isotropic macroscopic characteristics.

5.2 Structural Feature Level: There are microscopic-scale density fluctuations within the ether sphere itself; it has a dynamic structure formed through self-organization; it can support wave propagation and energy transfer.

5.3 Formation Mechanism of the Electron Structure: The continuous self-rotation of the ether sphere generates stable angular momentum; the periodic motion of the point photon forms standing wave mode; the synergistic action of the two maintains the stability of the electron's orbital motion.

5.4 Correspondence of Physical Properties: The self-rotation motion of the ether sphere corresponds to the spin property of the electron; the surface vibration mode explains the charge effect; the overall configuration determines the mass attribute.

This electron theory model provides a more intuitive physical picture and also offers a new perspective for understanding quantum phenomena.

5.5 Physical Explanation of the Wave-Particle Duality of Electrons

The wave-particle duality of electrons precisely stems from this complex motion mode. When observing electrons from the perspective of particles, what we see is a specific discrete state of the motion of point photons around the ether sphere, reflecting the particle nature of electrons. For example, in electron scattering experiments, electrons interact with target materials in the form of discrete particles and leave discrete signals on detectors. This can be understood as capturing the manifestation of electrons as "particles"under specific observation conditions.

5.5.1 Source of Wave Nature

Point photons move in an S-shaped closed loop around the ether sphere. This motion generates a series of fluctuations in the ether space. Just as water waves propagate on the surface of water, the motion of point photons within the ether-sphere of an electron drives local disturbances in the ether space, forming a periodically changing wave. The characteristics of this wave determine the wave nature of electrons. In interference and diffraction experiments, the phenomena of wave superposition and interference exhibited by electrons are precisely due to the interaction between the waves generated by the motion of point photons in the ether space within the electrons. The self-rotationofthe ether sphere further modulates the frequency and wavelength of these waves, making the wave nature of electrons closely related to the state of the ether space.

5.2 Unity of Particle Nature and Wave Nature

The particle nature and wave nature of electrons are not independent of each other but are unified in the same motion form in the ether space. When we attempt to measure the particle nature of electrons through experiments, the observation process affects the state of the etherspace, causing the motion of

point photons within the electron-stoma tend to exhibit discrete particle characteristics. When we focus on the wave nature of electrons, the state of the ether space underexperimental conditions causes electrons to behave in a wavelike manner. This unified relationship is similar to the collapse of the wave function under different measurement conditions, except that here it is the interaction between the physical process and the etherspace that leads to the manifestation of different attributes of electrons.

VI. MECHANISM OF ELECTRON ELECTRIFICATION

Different combinations of the self-rotation direction of the ether-sphere within fundamental particles such as electrons, protons, and neutrons and the S-shaped closed-loop motion direction of photon particles lead to three situations: fundamental particles carrying positive charge, negative charge, or being electrically neutral. Usually, electrons carry negative charge, protons carry positive charge, and neutrons are electrically neutral. The formationofantiparticles such as positrons is due to the action of forces, which causes the self-rotation direction of the ether sphere within fundamental particles such as electrons and the S-shaped closed-loop motion direction of photon particles to change.

6.1 Electrification of Fundamental Particles

The self-rotation direction of the ether sphere is perpendicular to the S-shaped closed-loop motion direction of the photonparticle(there are two cases: right-hand rule and left-hand rule). The motion of the photon particle cuts through the self-rotation motion of the ether sphere, causing the fundamental particle to acquire a positive or negative charge (Figure 2). One fundamental particle carries one unit of elementary charge, with an electric charge of 1.6021898×10^{-19} coulombs.

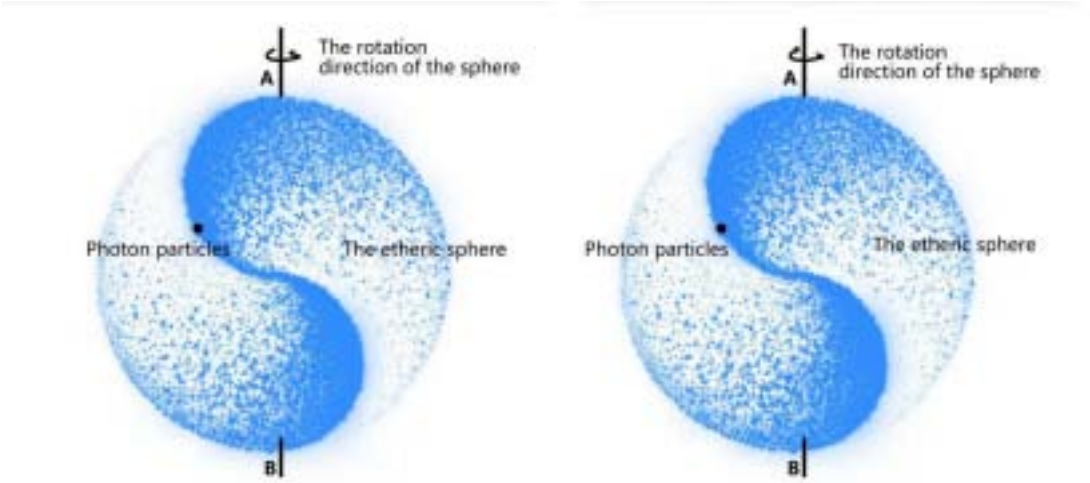

The case where elementary particles are charged

6.2 Electrically Neutral Fundamental Particles

When the self-rotation direction of the ether sphere is parallel to the S-shaped closed-loop motion direction of the photonparticle(there are two cases: the directions are the same or opposite), the motion of the photon particle cannot cut through the self-rotation motion of the ether sphere, thus no charge is generated. Such fundamental particles are electrically neutral (Figure 3).

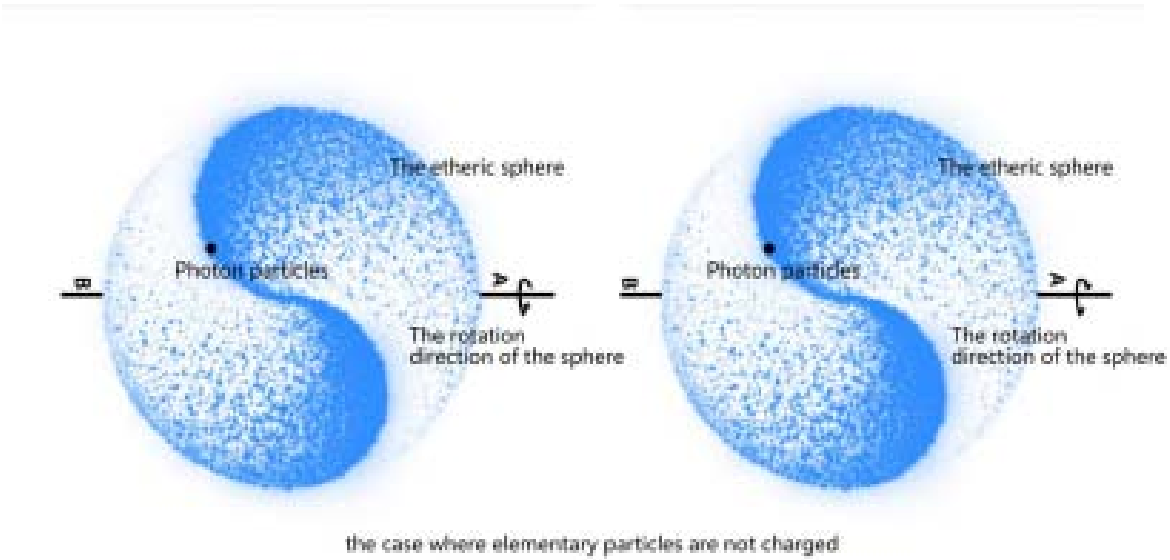

the case where elementary particles are not charged

VII. VERIFICATION CALCULATION BASED ON THE ELECTRON ETHER SPACESTRUCTURE MODEL

According to the above electron model (Figure 1), assuming the rest mass of the electron is m and the radius of the electron is r, then the wavelength of the electronλ is 2πr, the frequency of the electron² =hv. In this v is c / (2πr), and the energy of the electron Ee = mc paper, the modified Schwarzschild radius formula is Rs = GM/c². This paper points out that the Planck mass $M_P = \hbar c/G$(the specific formula is missing here). The derivation process is to combine the dimensional analysis of three basic constants (reducedPlanck constant ħ, speed of light c, and gravitational constant G)through mathematical methods. It lacks a profound physical mechanism explanation and does not clarify why the combination of these three specific constants has a mass meaning.

Based on the above premises, we attempt to verify relevant electron theoretical formulas based on the ether space structure model of electron wave-particle duality.

1. Derivation of the Compton wavelength formula $\lambda=h/(m_0c)$. Given the rest mass of an electron m, the radius of the electron, the particle energy of the electron Ee = mc ², which is equal to the ² = hv. Since the rest wave energy of the electron Ee = hv, that is, mc mass of the electron is the motion mass of the photon moving inan-shaped path around the surface of the ether sphere of the electron, and the radius of the photon from the center of the ether spheriser, then the angular momentum of the moving photon is always mcr, which is equal to the reduced Planck constant ħ. Given that the frequency v of the electron is c / (2 π r), substituting it intothe² = hv, we get mc equation mc²=hc/(2πr); simplifying gives mcr=h/(2 π); adjusting further gives h/(mc)=2πr. Since the wavelengthλ of a stationary electron is 2πr, the formula can be rewritten as λ=h/(mc).

In this formula, m is the rest mass of the electron, c is the speedoflight, h is the Planck constant, and λ is the wavelength of the stationary electron, which is completely consistent with the Compton wavelength formula. Therefore, it can be inferred that theCompton wavelength is the wavelength of a stationary electron.

2. Derive the Planck mass formula $M_P = \hbar c/G$. Accordingtotheabove derivation, it can be known that the wavelength formula of a stationary electron is the Compton wavelength formula. Then, the radius formula of a stationary electron is the Compton wavelengthλdivided by 2 π . After rearrangement, the radius formula of a stationary electron, i.e., the Compton radius formula, is $R_C = \hbar/(m_0c)$. Given that

the Compton wavelength formula is applicable to stationary fundamental particles, the Compton radius formula is also applicable to calculating the radii of stationary fundamental particles.

According to quantum theory, when the Compton wavelengths equal to the Schwarzschild radius, the derived mass is the Planckmass. However, based on the ether space model of fundamental particles such as electrons, these particles are not point-like but rather spinning ether spheres with rest mass and radius. Therefore, according to the Schwarzschild theory and formula, the corresponding quantum theory should be revised as follows: when the Compton radius $R_C = \hbar/(m_o c)$ of fundamental particles such as electrons is equal to the Schwarzschild radius $Rs = GM/c^2$, the derived mass is the Planck mass (the Schwarzschild radius formula here is the revised version in this paper). That is: $\hbar/(m_o c)=GM/c^2$. Since both m_0 and M on either side of the equation represent mass, they can be unified and represented by m. After rearranging and solving the equation for m, the result is: $m=\hbar c/G$,which is completely consistent with the Planck mass formula $M_P=\hbar c/G$. Thus, the derived Planck mass formula has clear physical significance.

3. Derive the formula for the minimum black hole mass of fundamental particles. According to the above derivation, the radius-formula of stationary fundamental particles such as electrons is $R_C =\hbar/(m_o c)$. When the radius of a fundamental particle equals thePlanck length $L_P= \hbar G/c^3$, the corresponding minimum black hole mass is also the Planck mass. By squaring both sides of the equation$\hbar/(m_o c)= \hbar G/c^3$ and rearranging, we obtain: $m= \hbar c/G$. Which is completely consistent with the Planck mass formula $M_P= \hbar c/G$.

It can be seen that, based on the ether space structure model of the electron, not only the Compton wavelength formula can be derived, but also the Planck mass formula with clear physical significance.

4. Refine the de Broglie Wavelength Formula. The de Broglie wavelength formula ($\lambda =h/p$) does not take into account the relativistic effects when particles move at high speeds. Consider an electron with a rest mass m_o that moves at a constant velocity in space after being subjected to a force. The relativistic mass of the electron is m. Starting from the relativistic energy-momentum relation, the total energy E and momentum p of a moving particle$in^2 = (pc)^2 + (m_o c^2)^2$. Expanding this formula gives: relativity satisfies: $E^2 + (m_o c^2)^2$. Rearranging terms, we get: $(mc)\ (mc^2)^2= (pc)^2 =(mv)^2 +^2 = (mc)^2 - (m_o c)^2$. Taking $(m_o c)^2$. By isolating terms, we obtain: (mv) the square root of both sides yields: $mv= mc^2 –m_o c^2$. The physical meaning of this formula is that the momentum of the moving particle p = mv is equal to the square root of the square of the intrinsic momentum (mc) of the moving mass minus the square of the intrinsic momentum $(m_o c)$ of the rest mass m_o. Therefore, the de Broglie wavelength formula $\lambda=h/p$ can be refined to account for relativistic effects as: $\lambda =h/mv) =h/ mc^2 – m_o c^2$.

Based on the refined de Broglie wavelength formula, it can be seen that this wavelength corresponds to the momentum generated by the spatial displacement motion of the particle, rather than the wavelength corresponding to the intrinsic momentum of the particle at rest. Therefore, the velocity v of the particle must satisfy: $0 < v < c.^2 = (mc)^2 - (m_o c)^2$, if When v = 0: According to the equation $(mv)^2 = (m_o c)^2$, and thus $m = m_o$. In this case, the v = 0, then (mc) particle is at rest, has no motion wavelength, and the de Brogliewavelength $\lambda = 0.^2 = (mc)^2 - (m_o c)^2$, we get When v = c: Substituting v = c into $(mv)\ m_o = 0$. In this case, the particle transforms into a photon, with zero rest mass and a moving mass m. Since photons are point particles without internal spatial structure, the wavelength associated with their motion is both the de Broglie wavelength and the photon's own wavelength, given by: $\lambda=hc/E$. Because m is the moving mass of the photon and $E=mc^2$, substituting into the photon wavelength formula gives: $\lambda=h/(mc)$.

VIII. FORMATION OF ATOMS BY FUNDAMENTAL PARTICLES SUCH AS ELECTRONS

From the formation of fundamental particles such as electrons, it is known that protons, neutrons, and electrons are all self-rotatingether spheres, with their photon particles moving in an S-shaped closed-loop motion along the surface of the ether sphere. Since ether can overlap and stack, it is hypothesized that atoms are structured as follows:

7.1 Structure of a Single-Electron Hydrogen Atom

For example, a hydrogen atom is formed by the mutual overlap of one proton's ether sphere and one electron's ether sphere. Due to the smaller mass of the electron, the volume of the electron's ether sphere is larger than that of the proton's ether sphere, and the density of the electron's ether sphere is lower than that of the proton's ether sphere. The radius of the S-shaped closed-loop motion of the photon particles of the electron is greater than that of the proton, equivalent to the electron undergoing S-shaped closed-circular motion around the proton. The overlap of the proton's and electron's ether spheres generates a strong force, stabilizing the structure of the hydrogen atom. Therefore, there is no need to worry about the electron falling onto the proton (Figure 4). Becausethedensity of the electron's ether sphere is lower, the binding force generated between the electron and the proton is weaker than the binding force between the proton and the neutron.

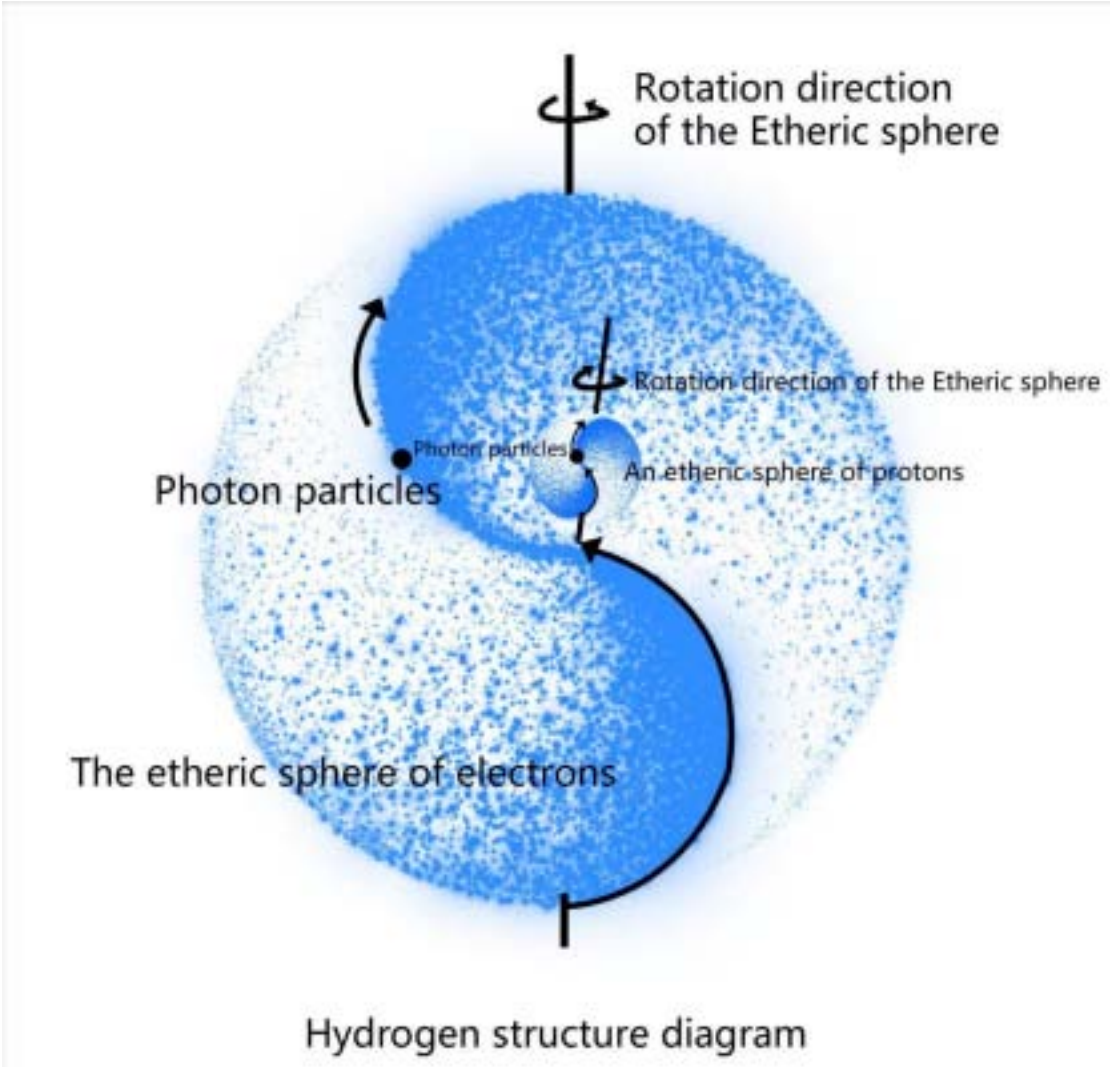

Hydrogen structure diagram

7. 2. Atomic Structure with Multiple Electrons

Atoms consisting of multiple protons, neutrons, and electrons are also structured according to this principle (Figure 5). The ether spheres of protons and neutrons overlap with each other to form the atomic nucleus, while the ether spheres of multiple electrons overlap with the atomic nucleus to form the atom. Within the atom: Electron ether spheres with smaller mass (positive energy) have larger volumes, lower negative energy density, and their photon particles move in an S-shaped closed-loop motion on the surface of the ether sphere. Their orbital paths are farther from the atomic nucleus.

Electron ether spheres with larger mass (positive energy) have smaller volumes, higher negative energy density, and their photon particles move in an S-shaped closed-loop motion on the surface of the ether sphere. Their orbital paths are closer to the atomic nucleus.

The closer the region is to the atomic nucleus, the greater the ether density; the farther the region is from the atomic nucleus, the smaller the ether density. Protons and neutrons, located at the center of the atom, form the atomic nucleus, where their photon particles moveinan S-shaped closed-loop motion around the surface of their respective ether spheres. Similarly, the photon particles of multiple electrons also move in an S-shaped closed-loop motion around the surface of their respective ether spheres, forming distinct orbital paths.

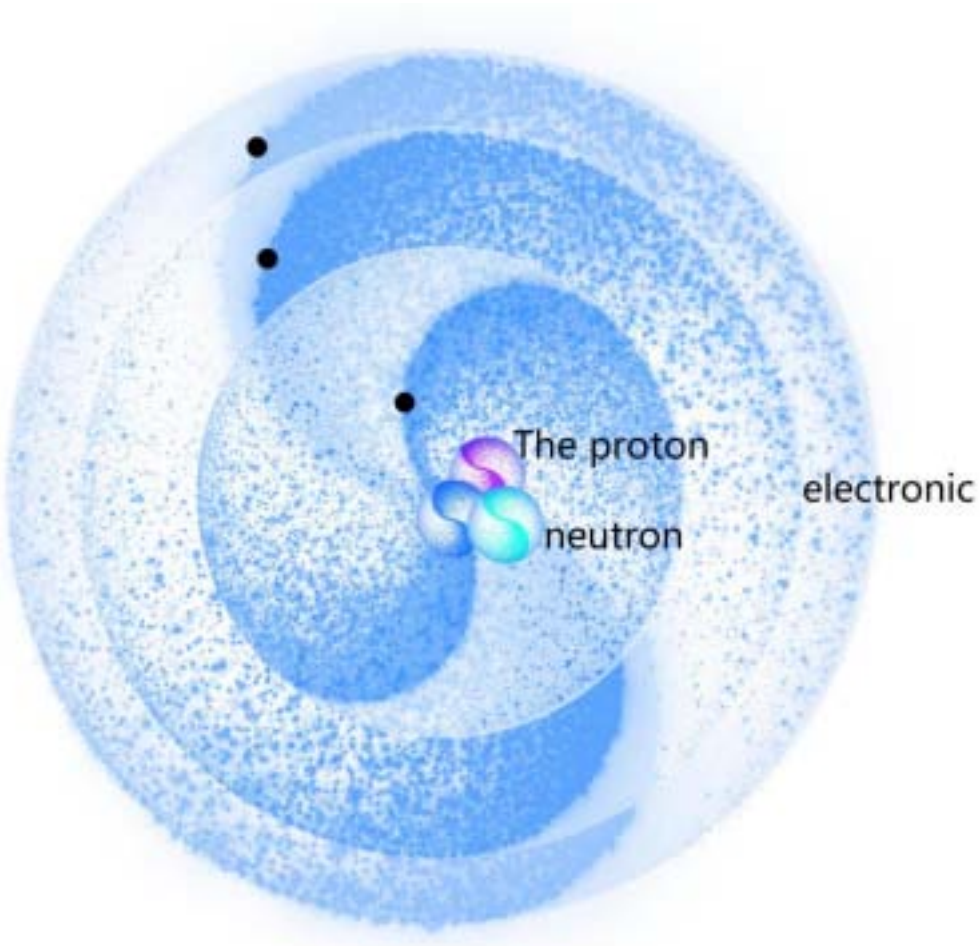

An atom composed of multiple protons, neutrons and electrons

VIII Summary

The hypothesis of the ether space model for the wave-particleduality of electrons intuitively explains the wave-particle duality of electrons, clearly defines the mass, radius, frequency, wavelength, and other properties of electrons, as well as their interrelationships. Based on this, the Compton wavelength and radius formulas arere-derived; the Schwarzschild radius formula under photonescape conditions is corrected; the Planck mass formula and the minimum black hole mass formula for particles are derived from a physical perspective; and the de Broglie wavelength formula is re-calculated, revised, and refined.

It should be noted that this hypothesis is based on the author's thought experiments and lacks empirical scientific experiments for verification. It is hoped that this paper can provide a new perspective for relevant scholars and make a modest contribution to their exploration and innovation in the fundamental theories of physics.

REFERENCES

1. Isaac Newton. *Philosophiæ Naturalis Principia Mathematica* [M]. The Commercial Press, 2006.
2. Albert Einstein. *Relativity: The Special and General Theory*[M]. Peking University Press, 2018.
3. Stephen Hawking. *A Brief History of Time* [M]. Taipei: Yiwén Publishing House, 1989.
4. Gottfried Wilhelm Leibniz. *Monadology* [M]. TheCommercial Press, 1975.
5. Cheng Jinjun. *Hypothesis about the Motion of Photon Space* (Open Access Library Journal, DOI: 10.4236/oalib.1105907).
6. Cheng Jinjun, Cheng Dian. *Several Conjectures About theExistence of the Ether* (European Journal of Applied Sciences–Vol. 9, No. 6, DOI: 10.14738/aivp.96.11240).

This page is intentionally left blank

Peculiarities of Electrodynamic Processes during Electric Explosion of Spiral Wires

L. P. Trofimova & A. F. Kolesnichenko

ABSTRACT

The features of the electric explosion of spiral-shaped conductors in the RLC discharge circuit are considered. It has been experimentally established that during the explosion of spiral-shaped wires in water, in contrast to the explosion in air, the secondary breakdown occurs along the spiral ionized channel due to the greater density of the environment, the lower expansion rate of the explosion products, and the compressive effect of the discharge channel of its own magnetic field. The nature of the discharge process is determined by the increase in the active resistance of the spiral plasma channel during its expansion. Due to the additional action of magnetic pressure generated during the explosion of the spirals, the force effect on electrically conductive objects located inside or outside the spiral increases, which can be used when distributing pipes in tube grids and loading samples with high pulse pressure. In addition, when changing the initial parameters of the spirals (number of turns, pitch, diameter) during their explosion in water, in the discharge circuit it is possible to observe the nature of the discharge from deeply oscillatory to deeply aperiodic, including obtaining a single pulse of discharge current for its use as a breaker for high-power electrical circuits.

Keywords: exploding wires, spiral shape, RLC discharge circuit, active and reactive resistance, circuit breaker, magnetic field strength, magnetic pressure, electric explosive expansion of tubes in tube sheets.

Classification: LCC Code: TK7811 QC794.3 TK5101

Language: English

Great Britain Journals Press

LJP Copyright ID: 925672
Print ISSN: 2631-8490
Online ISSN: 2631-8504

London Journal of Research in Science: Natural & Formal

Volume 25 | Issue 7 | Compilation 1.0

Peculiarities of Electrodynamic Processes during Electric Explosion of Spiral Wires

L. P. Trofimova[α] & A. F. Kolesnichenko[σ]

ABSTRACT

The features of the electric explosion of spiral-shaped conductors in the RLC discharge circuit are considered. It has been experimentally established that during the explosion of spiral-shaped wires in water, in contrast to the explosion in air, the secondary breakdown occurs along the spiral ionized channel due to the greater density of the environment, the lower expansion rate of the explosion products, and the compressive effect of the discharge channel of its own magnetic field. The nature of the discharge process is determined by the increase in the active resistance of the spiral plasma channel during its expansion. Due to the additional action of magnetic pressure generated during the explosion of the spirals, the force effect on electrically conductive objects located inside or outside the spiral increases, which can be used when distributing pipes in tube grids and loading samples with high pulse pressure. In addition, when changing the initial parameters of the spirals (number of turns, pitch, diameter) during their explosion in water, in the discharge circuit it is possible to observe the nature of the discharge from deeply oscillatory to deeply aperiodic, including obtaining a single pulse of discharge current for its use as a breaker for high-power electrical circuits.

Keywords: exploding wires, spiral shape, RLC discharge circuit, active and reactive resistance, circuit breaker, magnetic field strength, magnetic pressure, electric explosive expansion of tubes in tube sheets.

Author α: Institute of Pulse Processes and Technologies of the National Academy of Sciences of Ukraine, Nikolaev, Ukraine, 54018.
σ: Ispat Inland Ins. 3001 USA, E.Colubus Drive, East Chicago, In. 46312.

I. INTRODUCTION

The phenomenon of electrical explosion of conductors, which has been widely studied since the middle of the last century, has found practical application in various branches of industry [1]. One of the most developed and implemented in production can be called the deformation and pressing of pipes in pipe lattices, in particular in heat exchangers of nuclear power plants [2,3], in which the electric explosion of spiral wires was used. In works [4, 5] assumptions were made about the need to take into account the electromagnetic forces that arise when the discharge current flows through the spiral channel formed as a result of the electric explosion of wires of the corresponding shape during the explosion of spirals.

For the first time, possible changes in the distribution of the intrinsic magnetic field during the explosion of spiral-shaped wires in a vacuum were presented in the work [6], where it was shown that the current flows along the spiral in the first.

Stage of the discharge, when energy is introduced into the wire for the explosion, and the magnetic field strength inside it is determined by the number of ampere turns. This stage in the experiment lasted for about 10 mcs, after which a breakdown occurred between the turns with their overlap by the discharge current. The speed of movement of the explosion products in a vacuum calculated in the work was 10^3 m/s, and the maximum magnetic field strength was 10^5 A/m.

The present work sets the task of studying the electrodynamic processes accompanying the spiral electric explosion, as well as their influence on the magnitude of the force interaction with the objects of processing. For this purpose, experimental studies were conducted on the features of the electric explosion of spiral wires compared to the linear one in media of different density. The influence of the self-magnetic field of exploding spirals on the electrical characteristics of the discharge process was considered. High-speed photography, measurement of electrical characteristics (current, voltage) in the RLC discharge circuit, and measurement of the magnetic field intensity inside exploding spirals using a special probe in air and water were carried out. During the experiments, the following parameters for the reference points were changed: electrical capacitance C = 1 ÷ 30 mcF, discharge circuit inductance L_o = 0.9 - 5.02 mcH, capacitor charging voltage U_o = 40 - 50 kV, length of exploding aluminum wire l_{wir} = 145, 300, 750 mm, wire diameter in all cases was d_{wir} = 0,5 mm. The diameter of the spirals made of wires of the specified length varied in different series of experiments within the range d_{sp} = 2 - 42 mm. The number of turns N and the pitch of the spirals p were selected in accordance with the expressions: $N = l_{wir} / \pi d_{sp}$; $p = l_{sp} / N$, where lwir is the length of the wire, mm; l_{sp} is the length of the spiral, mm. The length of the spirals was l_{sp} = 30 and 40 mm. Thus, these parameters varied within the limits of N = (1 - 30) tur, p = 1 - 12 mm. The spiral with a diameter of 42 mm was a helically bent wire with a length of 145 mm, placed between the electrodes at a distance between them of l_{sp} = 30 mm, which corresponded to one turn, and the magnetic field inside it was minimal with the chosen initial parameters of the experiments.

The influence of the density of the surrounding environment on the nature of the explosion processes and the flow of the discharge current can be seen in Fig. 1, which shows the results of shooting spiral explosions in air and water using a high-speed photo recorder.

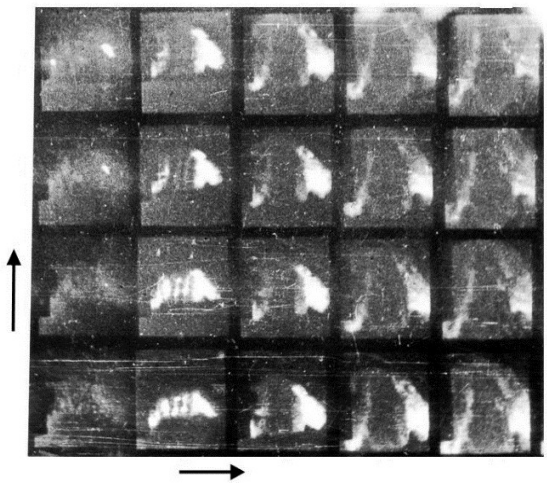

a

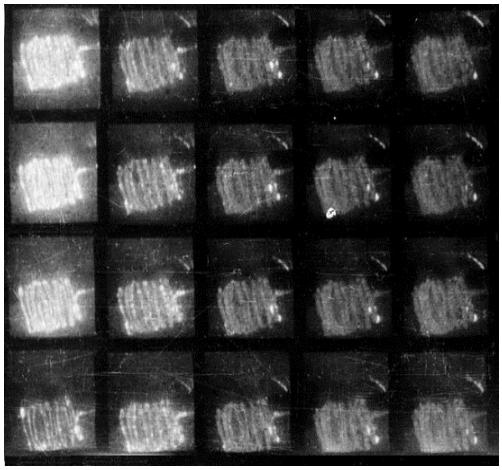

b1) Frames 1 – 20 b1) Frames 1 – 20

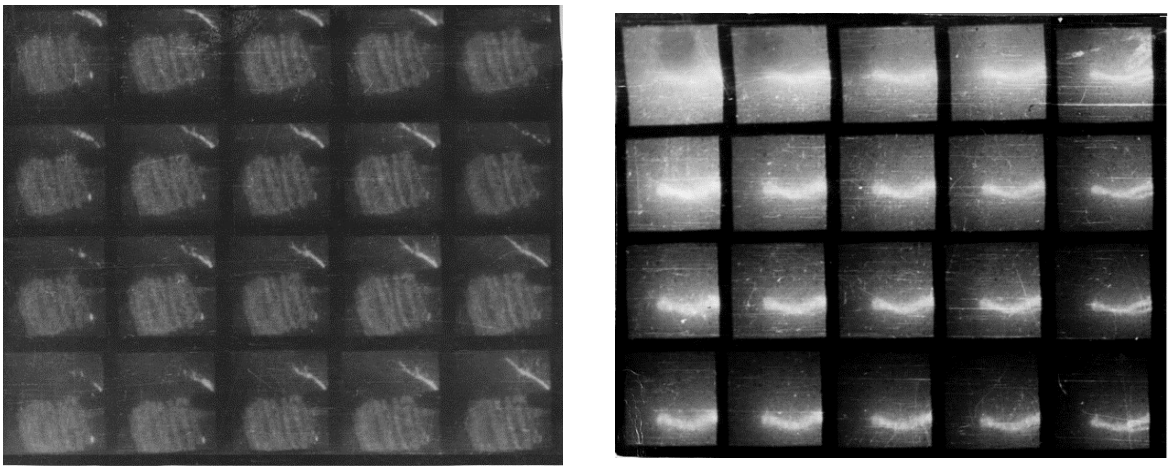

b2) Frames 25 - 44 c)

Fig. 1: Results of high-speed photography of the processes of electric explosion of spiral wires C = 9 mcF, L_o = 3.1 mcH. a) spiral wire in air U_o = 40 kV, d_{sp} = 7 mm, N = 6 tur, l_{sp} = 40 mm, l_{wir} = 145 mm, V_r = 1500 m/s, time between frames Δt = 2 mcs; b1), b2) spiral wire in water U_o = 42 kV, d_{sp} = 26 mm, N = 9 tur, l_{wir} = 750 mm, l_{sp} = 40 mm, V_r = 185 m/s, Vz = 30 m/s , Δt = 0.4 mcs; c) Overlap between spiral turns, linear discharge configuration U_o = 44 kV, V_r = 110 m/s, Δt = 0.4 mcs.

Fig. 2 shows the corresponding Fig. 1 a),b1),b2) measured in experiments changes in currents and magnetic field strengths in the center of the spirals.

From Fig. 1, 2, the following conclusions can be drawn. Before the beginning of the second stage of the discharge, during the melting and evaporation of the wires, their spiral shape is preserved in both environments. In this case, a characteristic current drop is observed, caused by the pressure of the explosion products (Fig. 2a, b). Further, differences are observed both in the expansion rates of the explosion products (Fig. 1) and in the nature of the currents flowing during this, as well as the pulses of magnetic field strengths (Fig. 2c, d).

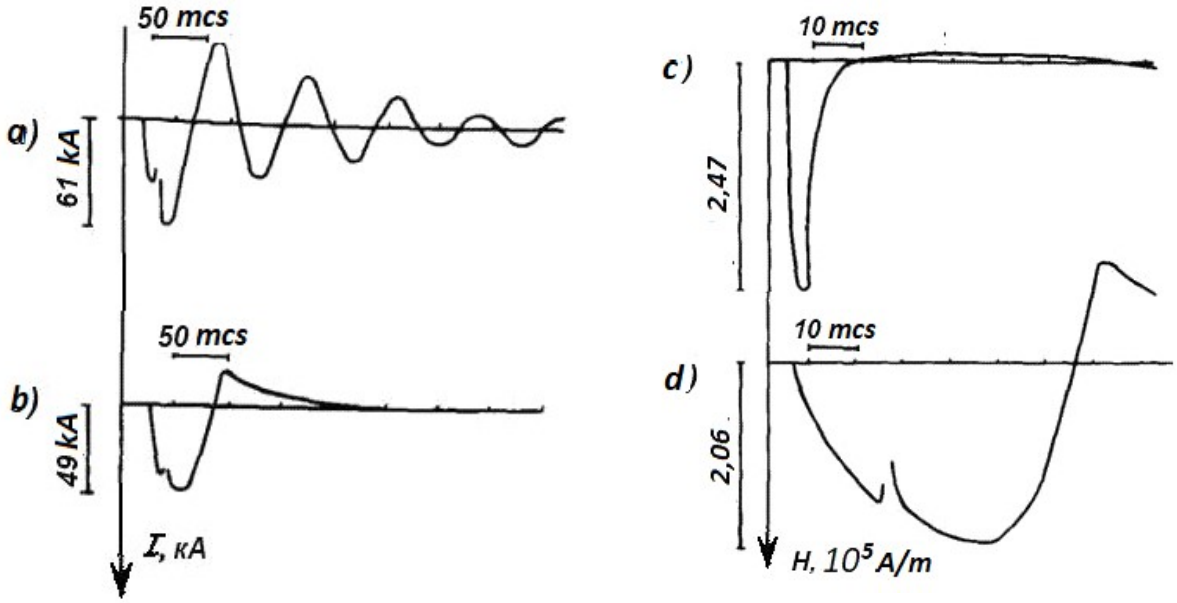

Fig. 2: Oscillograms of the discharge current I (a, b) and the corresponding magnetic field strength H (c, d) during the explosion of spirals in air and water.

For the explosion of the spiral in water, the nature of the current, all other things being equal, changed to a pulse with a surge of reverse polarity, aperiodically decaying (Fig.2b). In this case, the magnetic field intensity pulse corresponds in shape to the discharge current pulse. Its amplitude value, measured in the center of the spiral, is H_{max} = 2,06.10^5 A/m. V_r = 185 m/s. The current during an explosion in air (Fig. 2a) has an oscillatory nature with a half-period T/2 = 50 mcs, and the magnetic field strength pulse has the following parameters: amplitude H_{max} = 2,47.10^5 A/m, duration 7 - 8 mcs, pulse front 1 - 2 mcs. In air, the radial expansion velocity of the spiral explosion products is V_r = 1500 m/s, and the spiral shape of the wire is destroyed within 3 - 4 mcs from the beginning of the process (Fig. 1a). Table 1 shows the values of the expansion rates of the explosion products of spiral conductors in water and air, where it is shown that the expansion rates of the spiral discharge channel are different both in the radial direction of the spirals V_r and in the axial (along the axis) V_z.

Table 1: Experimental values of the expansion rates of the products of the electric explosion of spiral wires

№ in order	Initial data of the experiments	Explosion product expansion velocity (radial Vr, axial Vz), m/s
1	Spiral, explosion in water, d_{spo} = 7 mm, l_{wir} = 145 mm, N = 6 wir.	V_r = 205
2	Spiral d_{sp} (t), d_{spo} = 26 mm, l_{wir} = 750 mm, N = 9 wir.	V_r = 180
3	Linear discharge configuration	V_r = 110
4	Wire d_{wir}(t), d_{wiro} = 0,5 mm	V_z = 30
5	, Spiral, l_{sp} (t), l_{spo} = 40 mm	V_z = - 400 (from 0 to 30 mcs) V_z = 110 (>30 mcs)
6	Spiral, explosion in the air, d_{spo} = 7 mm, l_{wir} = 145 mm, N = 6 wir	V_r = 1500

For comparison, Table 1 shows the expansion rate of the linear discharge channel, caused only by the pressure of the explosion products V_r = 110 m/s, which is almost 2 times less than the increase rate of the spiral diameter, caused by the combined effect of both magnetic and gas-kinetic pressures on the expansion of the spiral plasma channel. The velocity values indicate an additional influence of the magnetic field concentrated inside the spiral on the radial velocity of its expansion. For identical experimental conditions, judging by the radial expansion velocities (180 m/s for the spiral and 110 m/s for the linear channel), the values of magnetic and gas-kinetic pressures on the turns of the spiral discharge channel are comparable in order of magnitude, therefore the additional effect of magnetic pressure on the turns from inside the spiral leads to an increase in the radial expansion velocity by almost 2 times. Comparison of the radial velocities of the coil expansion in the axial direction of the spiral, along its axis (respectively, 30 m/s and 110 m/s), indicates the deceleration of the discharge channel expansion in this direction. In addition, the conclusion suggests itself that from the beginning of the discharge process to the second stage of the discharge in both media (air, water) the spirals retain their shape. In air, at the end of the first stage, the spiral shape is destroyed due to the high speed of the explosion products, and the second stage becomes linear. In this case, the current oscillogram has an oscillatory nature (Fig. 2a). The duration of the magnetic field intensity pulse inside the spiral in air corresponds to the explosion time before the onset of the second stage of the discharge. And the nature of the discharge current is determined by the RLC parameters of the discharge circuit, in this

case it is a deeply oscillatory process. It is precisely this nature of the processes that the authors observed during the explosion of spirals in a vacuum in [6].

Unlike an explosion in air, in water the current flows through a spiral channel during the entire discharge process, including the second stage. As in any solenoid, two components of the force of electrodynamic interaction begin to act on it. Axial F_z, which tends to compress the solenoid from the ends to the center, and radial F_r, which tends to break the turns in the radial direction. As a result of the action of F_r, the radial expansion rate of the spiral channel increases compared to the linear one. The decrease in the channel expansion rate in the axial direction of the spiral indicates the deceleration of the discharge channel due to magnetic forces during the interaction of the current in the turns of the spiral. This is evidenced by a slight decrease in the total length of the spiral channel within 30 mcs from the beginning of the discharge process (see Table 1). Further expansion of the spiral in this direction occurs with the expansion of the outer turns of the spiral on both sides due to gas-kinetic pressure.

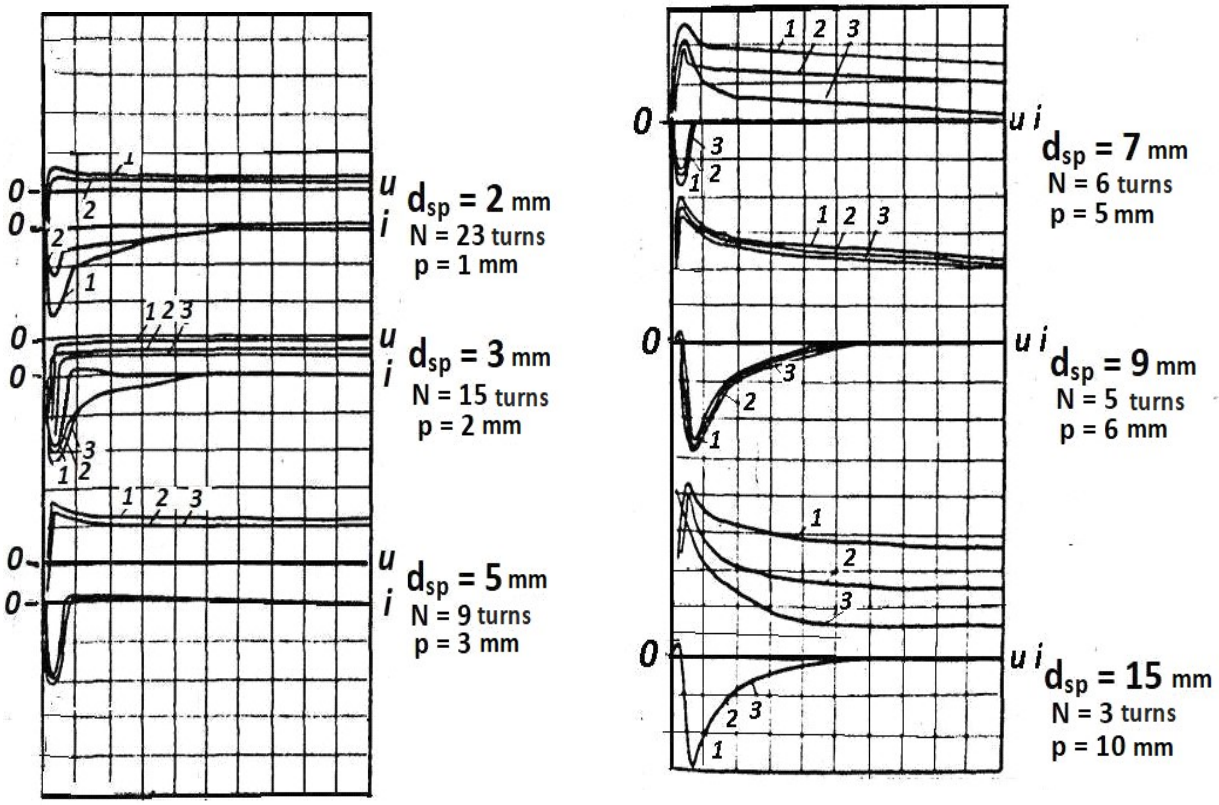

Fig. 3: shows oscillograms of current and voltage during the explosion of spirals in water.

Fig. 3 Oscillograms of current and voltage during the explosion of spirals in water. l_{wir} = 145 mm, l_{sp} = 30 mm. Scales: current i - 3 kA /div, voltage u - 4.4 kV/div, time t - 10 mcs/div. U_o = 40 kV, C = 3 mcF, L_o = 3.1 mcH

The spirals are made of wires of the same length l_{wir} = 145 mm. The diameter of the spirals varied within d_{sp} = 2 - 15 mm. Three experiments were conducted per point. It should be noted that the data scatter is satisfactory for both current and voltage. In all cases, when the spirals explode, a pattern is observed - the voltage does not drop to zero simultaneously with the current, but continues to be applied to the gap. This residual voltage is quite high and in some cases is more than half the voltage initially applied. This fact indicates that the resistance of the discharge channel during the explosion of spiral-shaped wires in water increases so much that it slows down the discharge process after the explosion. This fact indicates that the resistance of the discharge channel during the explosion of spiral wires in water increases so much that it slows down the discharge process after the explosion.

The active resistance of the discharge circuit, taking into account the resistance of the spiral plasma channel in water R (t), was calculated using expression (1), when the cross-section of the plasma channel was approximated by an ellipse, and the rates of change in the dimensions of the spiral were taken from the experiment. The change in electrical conductivity was taken into account by means of the action integral until the moment of evaporation of the conductor [7, 8]:

$$R(t) = R_0 + \frac{N(d_{sp} + 2V_{sp}t)}{\sigma_0\{(r_{wir} + V_1 t)(r_{wir} + V_z t)\}} \exp\{b/\sigma_0 \int_0^t i^2 dt\} \quad (1),$$

where: R_o is the active resistance of the circuit, Ohm (calculated based on the degree of current attenuation on the oscillogram of a short circuit of the circuit $R_o = 2\Delta L_o$, where Δ is the degree of short circuit current attenuation); N is the number of turns of the spiral; dsp, rwir are the diameter of the spiral and the radius of the wire; V_{sp} = 200 m/s is the experimental value of the radial expansion velocity of the spiral plasma channel; σ_o is the electrical conductivity of the material at 20° C; $(r_{wir} + V_1 t)$ is the semi-major axis of the elliptical cross-section of the expanding plasma spiral channel; V_1 = 100 m/s is the expansion velocity of the linear channel; $(r_{wir} + V_z t)$ is the semi-minor axis of the ellipse; V_z = 30 m/s is the expansion velocity of the spiral in the axial direction (along the axis); $b_{Al} = 2{,}15.10^{-9}$ is the thermal coefficient for aluminum; $\int i^2 dt = 1{,}09.10^{17}$ A² s m⁻⁴ is the action integral until the moment of conductor evaporation. The calculations were performed for the following initial parameters of the spirals: wire material - aluminum, l_{wir} = 145; 300; 750 mm, r_{wir} = 0,25 mm. The initial active resistance of the 145 mm long wire was 0.018 Ω. Calculations showed that for a spiral d_{sp}= 7 mm at N = 6 turns at the moment t = 5 mcs, R_{sp} = 3.8 Ω, and L_{sp} = 0.08 mcH (in the Table 2). The ratio of active Rt and reactive $R_r = \sqrt{[(L_o + L_{sp})/C]}$ resistances m = R_t/R_r is equal to m = 2.1, the nature of the current in the experiment is close to a single pulse. For a spiral d_{sp} = 26 mm, made of wire l_{wir} = 750 mm and N = 9 tur at R_{spo} = 0.097 Ω for t = 5 mcs, R_t = 16.1 Ω, L_{sp} = 1.2 mcH, and m = 10.9, which corresponds to the deeply aperiodic nature of the discharge current in the experiment.

Table 2 presents the initial data of the experiments, the results of calculating the change in the active resistance R_t, the inductance of the spirals L_{sp} for the time t = 5 mcs from the beginning of the discharge process, the active Rt, reactive Rr resistances and their ratio m = R_t/R_r, as well as the results of experiments on the observed current pulses during the explosion of spiral wires. As is known [9], with a ratio of active and reactive resistance in the RLC discharge circuit m = 2, a single pulse should be observed. At m < 2 the discharge is oscillatory, and if m > 2, the discharge should have an aperiodic character with a corresponding increase in the steepness of the pulse front and a decrease in its amplitude. The inductance of the discharge circuit, taking into account its change during the expansion of the spiral discharge channel after the explosion, was calculated using the method described in [10].

Table 2: Comparison of calculated and experimental parameters of the nature and degree of attenuation of the discharge current in the RLC circuit.

№ in ord.	Parameters of the discharge circuit and the exploding element (initial dimensions)	Calculation at t = 5 mcs				Experiment
		Active resistance of the	Discharge channel inductance	Reactance R_r, Ω	m= R_t/R_r	Current pulse character, front/fall,mcs

		discharge channel R_t, Ω, (R_t/R_o)	L_t, mcH, (L_t/L_o)			(I_{max} , kA)
1	2	3	4	5	6	7
1	Linear wire l_{wir} = 145 mm, d_{wir} = 0,5 mm, R_o = 0,018 Ω; L_o = 4,72 mcH, C = 9 mcF, U_o = 40 kV	0,7 (39)	0,08 (0,02)	0,73	0.93	Oscillatory half-period T/2 = 15 mcs, (I_{max} = 20 kA)
2	Spiral d_{sp} = 11 mm, l_{wir} = 145 mm, d_{wir} = 0,5 mm, N = 4 tur., R_o = 0,018 Ω, L_o = 5,02 mcH, C = 9 mcF, U_o = 40 kV	1.78 (99)	0.066 (0,013)	0.57	2,37	Single, 3,0/5,3; (30.2)
3	Spiral d_{sp} = 7 mm, l_{wir} = 145 mm, d_{wir} = 0,5 mm, N = 6 tur. R_o = 0,018 Ω, L_o = 3,21 mcH, C = 3 mcF, U_o = 40 kV	3,8 (211)	0.078 (0,24)	3.0	2,1	Single, 4,0/5,3, (7,8)
4	Spiral d_{sp} = 7 mm, l_{wir} = 145 mm, d_{wir} = 0,5 мм, N = 6 tur., R_o = 0,018 Ω, L_o = 4,1 mcH, C = 9 mcF, U_o= 40 kV	2,21 (123)	0,078 (0.82)	9,0	3,1	Aperiodic, 0/60,0, (10,2)
5	Spiral d_{sp} = 26 mm, l_{wir} = 750 mm, d_{wir} = 0,5 mm, N = 9 tur., R_o = 0,18 Ω, L_o = 4,1 mcH, C = 9 mcF, U_o = 40 kV	8,47 (470)	1,05 (0,26)	0.77	1 0.9	Aperiodic, 0/60,0, (5,0)
6	Spiral d_{sp} = 14 mm, l_{wir} = 300 mm, d_{wir} = 0,5 mm, N = 6 tur., R_o = 0,039 Ω, L_o = 4,85 mcH, C = 30 mcF, U_o = 50 kV	2,26 (58)	0,21 (0,04)	0,41	5,6	Aperiodic, 0,0/20, (30,0)

From the results of explosion of long wires 760 and 300 mm, twisted into spirals, presented in the table, it can be concluded that in the case when the explosion itself does not occur, but overheating of conductors characteristic of such wires is observed, after the discharge in water a plasma or liquid metal spiral is formed with a characteristic change in the degree of attenuation of the discharge current towards aperiodicity. In calculations after t = 5 mcs from the beginning of the discharge process, an increase in the active resistance of the circuit is observed due to the expansion of the spiral with an increase in the length of the discharge channel by 40 - 470 times. At the same time, the total inductance L_o + L_{sp} increased by this time by 1,1 - 1,3 times. This confirms the initial assumption that the main role in changing the nature of the discharge process during the explosion of spirals is played by the growth of the active resistance of the discharge channel, which grows due to the increase in its

length. Comparison of calculations and experiments shows their satisfactory agreement. The use of spirals with a number of turns N = 4 - 9 tur for RLC circuits in experiments made it possible to obtain single current pulses with a front of 3 - 5 mcs, which suggests the possibility of using them as circuit breakers for energy sources with an amplitude current of the order of tens of kA. Another example of the use of a magnetic field of the order of $H = 10^5$ A/m, observed during the electric explosion of spiral wires in water, can be devices for compression of magnetic flux [11].

The discharge current in the range of spiral diameters of 7 - 10 mm (N = 6 - 4 tur) has an aperiodic character or the character of a single pulse. With smaller diameters and, accordingly, a larger number of turns and a smaller pitch, a complete or partial overlap between them by plasma occurs, the discharge takes a linear form, the magnetic field strength decreases and, accordingly, as experiments have shown, the current has an oscillatory nature. With large spiral diameters (more than 10 mm), the number of ampere turns decreases with a corresponding decrease in the magnetic field strength inside the spiral. The current character is again oscillatory. It should be noted that the effectiveness of the impact on the object loaded during the explosion of the spirals, for example, a deformable pipe, is maximum in the region of spiral diameters d_{sp} = 7 - 10 mm, N = 4 - 6 tur, when the magnetic field inside the spiral is maximum, the rate of expansion of the spiral is also maximum, which is preferable in technological processes of metal pressure treatment using cylindrical geometry of deformable parts. However, it should be borne in mind that additional requirements should be imposed on the high-voltage insulation of the process unit in order to avoid discharges on the tube sheet and ineffective impact on the deformable pipe.

In accordance with the amplitude values of the discharge current and the values of the maximum magnetic field strength in the center of the spirals, measured in the experiments, the magnetic pressure Pm on the turns of the exploding spiral was calculated using expressions (2), (3) [8]:

$$P_m = \mu_0 H^2_{z(0)} / 2f, \quad (2)$$

where: $f = Nd_{wir} / l_{sp}$ is the winding density of the spiral; $H_{z(0)}$ is the magnetic field strength in the center of the spiral.

$$H_{z(0)} = 1/4 H_F \operatorname{ctg} 2P/\pi\, d_{SP} [(2a/l_{sp})^2 + 1]^{-1/2} \quad (3)$$

Fig. 4 shows the results of calculations of the magnetic pressure inside the spirals on their turns based on the values of the measured discharge current (curve 1a), as well as on the measured values of the magnetic field strength (curve 1b). Dependence 2 takes into account the overlap between the turns. Dependence 3 is hypothetical under the assumption that there was no overlap between the turns.

Dependence 2 takes into account the overlap between the turns. It is evident that the value of magnetic pressure increases due to the change in the shape of the spiral and the number of turns by almost an order of magnitude and reaches values of $P_m = 10^8$ Pa. Under the influence of this pressure, the rate of expansion of the spiral increases, the total length of the discharge channel increases and, accordingly, its active resistance. The value of magnetic pressure for the experimental conditions is comparable in order of magnitude with the hydrokinetic pressure developed during the actual electric explosion. Therefore, one can assume, for example, the following mechanism of tube distribution in tube grids during the explosion of spiral wires. At the beginning of the discharge current flow, primary deformation of the loaded pipe due to magnetic forces, and then additional impact action due to hydraulic shock compacts the pipe expansion site. Thus, the quality of pipe expansion is improved.

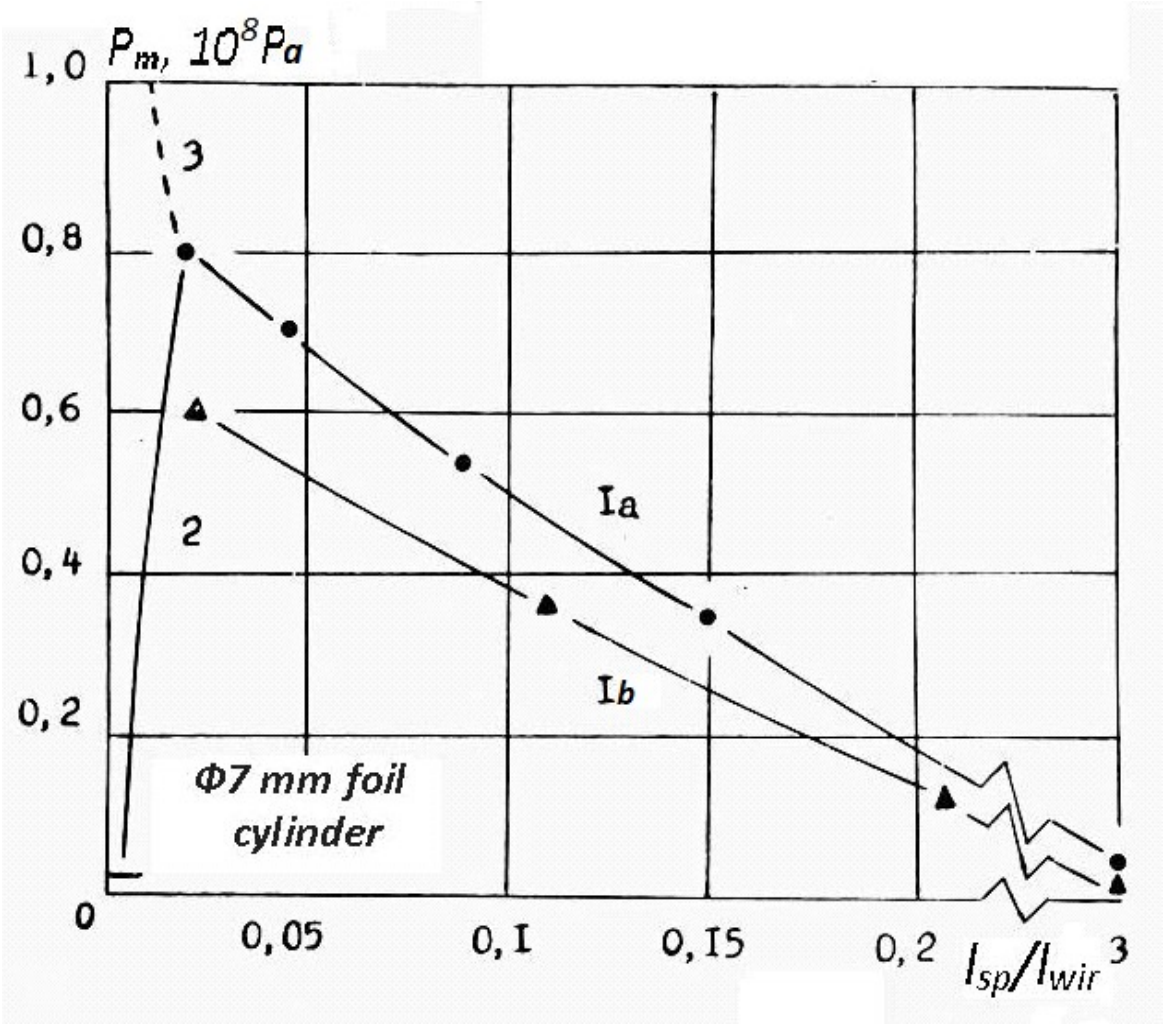

Fig. 4: Dependence of magnetic pressure on the turns of the spiral on its diameter. 1a - calculation based on the measured current amplitude; 1b - calculation based on the measured magnetic field strength; 2 - taking into account the overlap between the turns; 3 - without taking into account the overlap between the turns.

As an example of the effect of the self-magnetic field of a spiral exploding wire in water, loading was carried out on graphite samples (far left in Fig. 5) with the following dimensions: length 40 mm, diameter 5 mm. The sample was placed in a copper tube (second from the left in this figure) with a wall thickness of 1 mm. The sample was wrapped in aluminum foil with a thickness of 40 mcm, which after loading exploded due to the currents induced in it, thereby providing additional gas-dynamic pressure acting on the sample [12].

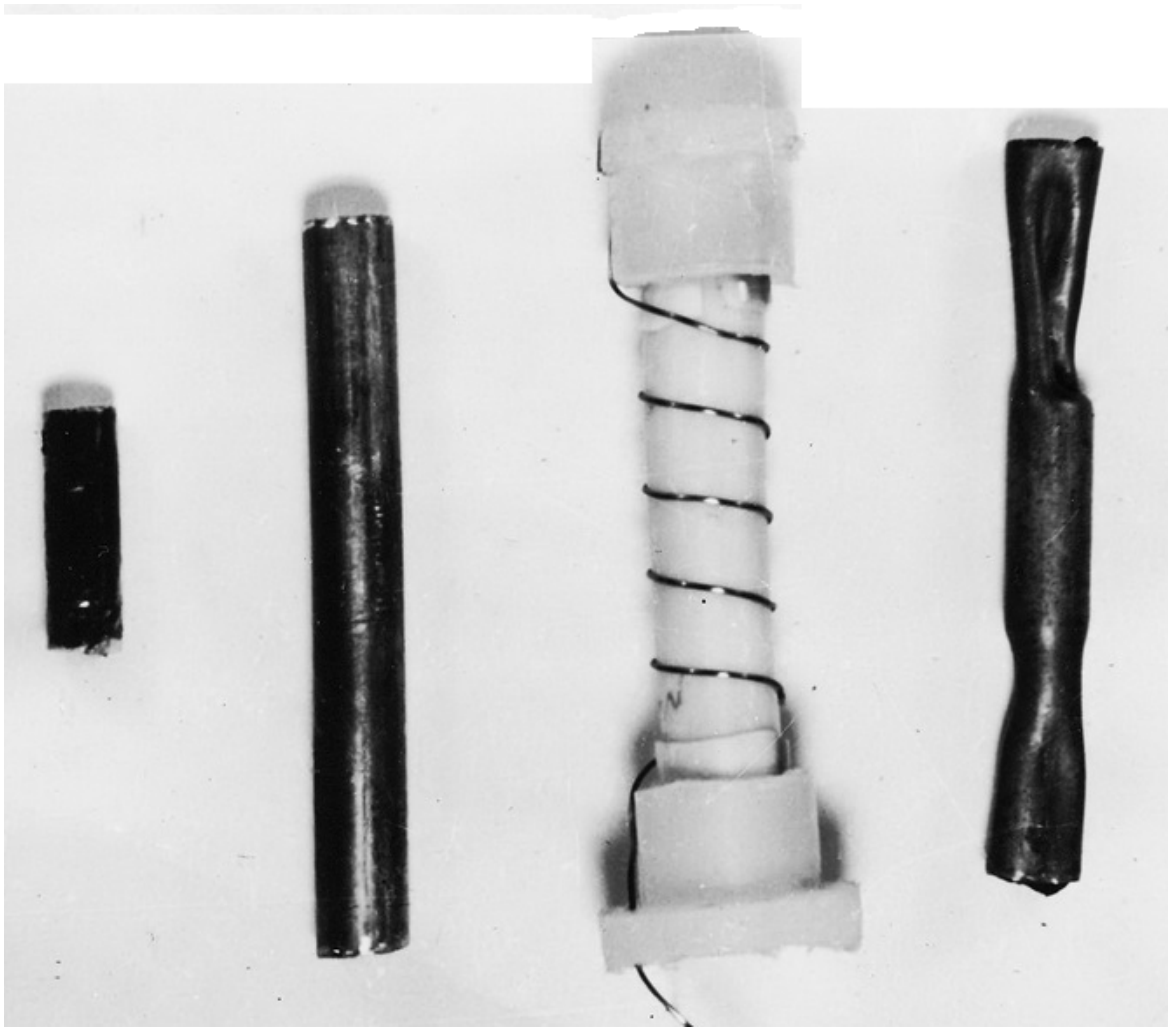

Fig. 5: Result of loading a graphite sample placed inside a copper tube during electric explosion of a spiral wire in water. Sample, tube and capsule before treatment and sample inside the tube after loading.

II. CONCLUSIONS

1. A spiral-shaped discharge plasma channel, formed as a result of an electric explosion in water of a wire of the corresponding shape, represents a variable resistance, increasing during the discharge process in comparison with its initial resistance by several orders of magnitude due to an increase in the length of the discharge channel.
2. By changing the initial parameters of the spiral wire (wire length, number of turns, spiral pitch), it is possible to obtain discharge characteristics from deeply oscillatory to deeply aperiodic at the secondary stage, including obtaining a single current pulse that can be used to open high-power electrical circuits.
3. When a spiral wire exploded in water, a magnetic field strength of about 10^5 A/m and a pulsed magnetic pressure on a sample of about 10^8 Pa in a volume of cubic cm with a duration of up to 100 mcs were recorded. A magnetic field with such parameters and in such a volume can be used in metal deformation technologies, loading samples with high pressure, and also as a source of initial magnetic flux during magnetic cumulation.

ACKNOWLEDGEMENTS

The authors are grateful to PhD of EngS Telyashov L.L. for useful discussion and to Cand. Of EngS. Poklonov S.G. for assistance in conducting the experiments.

REFERENCES

1. V. Chase "Brief review of research on exploding wires", Exploding wires, Moscow, IL. 7-10 (1963).
2. P.A. Andreev, D.I. Gremilov, E.D. Fedorovich " Heat exchangers of nuclear power plants", Moscow, Sudostroenie, 352 p.(1969).
3. B.Ya. Mazurovsky, Zh.N. Ishchenko, B.Ya Konvisher " Installations for electrohydro pulse flaring of tubes in tube sheets". Chemical and Oil Engineering, No. 2, 29-30 (1977).
4. L.P. Trofimova " On the electrical explosion of spiral wires inside a conducting cylindrical tube". Electronic Processing of Materials, No. 1, 38-41 (1976).
5. Zh.N. Ishchenko, L.Yu. Gulyaeva " Study of underwater electrical explosion of spiral-shaped wires". Electronic Processing of Materials, No. 2, 53-58 (1979).
6. I.R. Kvartskhava, A.F. Bondarenko, A.A. Chernov, "Electrical explosion of spiral wires in vacuum", Zhurnal eksperimental'noi i teoreticheskoi fiziki, vol. 35, No. 4, 911-916 (1958).
7. R. Rompe, W. Weizel "About electric explosions" , Z. Physik, 122, 636-639 (1944).
8. L.P. Trofimova, A.F. Kolesnichenko, P.P. Malyushevsky, G.A. Trofimov " Influence of magnetic field of current of exploding spiral wires on amplitude and degree of attenuation of discharge current", Problems of technical electrodynamics, Kyiv, No. 63, 67-71 (1977).
9. V.Ya. Ushakov " Pulsed electrical breakdown of liquids", Tomsk, Tomsk University, 255 p. (1975).
10. P.L. Kalantarov, L.A. Zeitlin " Calculation of inductances", Moscow, Energiya, 230 p. (1970).
11. L.P. Trofimova, A.F. Kolesnichenko, P.P. Malyushevsky, G.A. Trofimov "Obtaining high pulse pressures in devices of cylindrical geometry based on electrodynamic interaction of currents", Improving the quality of electrical energy, Kyiv, Naukova Dumka, 91-95 (1978).
12. A.I. Vovchenko V.V. Shamko, P.P. Malyushevsky, L.P. Trofimova " On the selection of design schemes and modes of electrical explosion for the synthesis of dense modifications of carbon", Abstracts of reports of the conference on pulse methods of materials processing, Minsk, 48 - 49 (1978).

This page is intentionally left blank

Evolution Sucks

Volker w. Thürey

ABSTRACT

The article deals with evolution and the environment. I assume the unproven claim that all life is generated through evolution. In the chapter titled "Evolution Sucks" I demonstrate that it can sometimes have negative consequences. Although there is no alternative academic explanation, I illustrate some of the 'disadvantages' of Darwin's theory.

In the final chapter "The Glut Society" I reference some older books on climate change and the environment in general.

Keywords and phrases: evolution; climate change.

Classification: LCC Code: QH366.2

Language: English

Great Britain Journals Press

LJP Copyright ID: 925673
Print ISSN: 2631-8490
Online ISSN: 2631-8504

London Journal of Research in Science: Natural & Formal

Volume 25 | Issue 7 | Compilation 1.0

Evolution Sucks

Volker w. Thürey

ABSTRACT

The article deals with evolution and the environment. I assume the unproven claim that all life is generated through evolution. In the chapter titled "Evolution Sucks" I demonstrate that it can sometimes have negative consequences. Although there is no alternative academic explanation, I illustrate some of the 'disadvantages' of Darwin's theory.

In the final chapter "The Glut Society" I reference some older books on climate change and the environment in general.

Keywords and phrases: evolution; climate change.

I. INTRODUCTION

In line with Darwin's theory, I assume that all life forms arise through evolution. Of course, this assumption is not provable.

II. THE CREATIVE IMPULSE

First, I discuss a book [1], titled "Der schöpferische Impuls" (The Creative Impulse) by the German biologist Josef H. Reichholf. I found this book in an antiquarian bookshop. One of its statements is that the progress of life was primarily driven by global crises. I believe that this is incorrect. I reject the hypothesis that evolution was driven forward by global changes. My reasoning is that sexuality is the last activity animals would abandon. Sex nearly always leads to reproduction. This has the consequence that evolution continues despite any crises.

Despite my disagreement with some of its hypotheses, I found this book very stimulating and thoughtprovoking.

III. OPTIMISM IS STUPID

As an example, let's consider an important food fish, the Atlantic herring (Clupea harengus). A herring can live up to 20 years (if it is not eaten first). Over its lifetime, a female fish can spawn up to 1000000 eggs. Most of the eggs were eaten, but some managed to hatch. From these, most were eaten, but some survived. I am sure that herrings don't think about their situation, but if they could, they would feel very optimistic. They might think something like "Up to now, I have survived. This means that I am very clever. I also will avoid being killed in the future."

Of course, their survival was only a matter of luck.

IV. EVOLUTION SUCKS

The progress of evolution happens by accident. Evolution neither has direction nor purpose. There is evolutionary progress only through reproduction. In recent decades, researchers have gained a better understanding of how it works. Specially, how the genetic material is transported.

However, evolution has some 'disadvantages'. Here I present a few.

First, I want to mention the book by the German forester and author Peter Wohlleben: "Das geheime Leben der Bäume" (The secret life of the trees) [2]. It was published in 2015, and it was a huge success in Germany.

Wohlleben describes trees are caring, social beings. He writes that older trees supply nutrients to younger trees through their roots. I believe that the seemingly solicitousness is nonsense. There is another explanation for the observation. Perhaps the young trees are simply para sites. The adult trees might have an excess of nutrients. Therefore, they did not develop any defence against the younger trees. But the name "caring trees" sounds much more appealing for a socially-minded human.

According to the theory of Darwin, all life forms are generated by evolution. Yet when in radio or TV something is discussed about evolution, it is portrayed as a mysterious process, guided by a kind of secret force. Some people think that evolution has a direction, i.e. simpler life forms evolve automatically into sophisticated ones. This is nonsense. The development of life's diversity is largely a matter of chance. Creatures develop intelligence only if it provides an advantage in the struggle for survival.

In Darwin's theory, I miss the word "death". That means, I miss the portrayal of how evolution works.

On one hand, evolution is incredibly creative. It generates complex organs, for instance, an eye. On the other hand, it is cruel and merciless. Nature often eliminates individuals who aren't well-adapted. Indirectly this is expressed by Darwin's slogan "Survival of the fittest". Usually an anomaly is 'punished' by death.

Evolution advances because only those whose genetic material is passed on survive. It is at the cost of those who don't. In fact, it would be enough just to prevent certain individuals from reproducing. Evolution achieves this by killing those who are less fit.

In this light, modern medical care runs contrary to evolution. The progress of medical science, which saves life and reduces suffering, goes against the brutal mechanism that drives natural selection. From an evolutionary perspective, medical progress is a cul-de-sac.

Evolution advances through death. One important requirement for the development of human ity has been the poverty of human societies. Poverty ensures high mortality rates — through starvation and disease — which, in turn, drives evolution. Seen in this way, the fight against poverty might seem counterproductive, as it interferes with this natural process. Ironically, when poverty is reduced and population numbers increase, poverty tends to reappear due to limited resources.

For the majority of people there is only one guarantee against poverty in seniority. They must have as many children as possible. Some survive and facilitate their old parents.

In a human society with 'good' circumstances, people propagate as long as it turns into 'bad' circumstances, or, in other words, people propagate as long as the number of fatalities is equal to the number of newborns.

It is a fact that, in all species without an exception, the number of offspring far exceeds what's necessary for species preservation. Since the number of individuals of a species remains relatively stable, the logical consequence is that most animals die in younger age, i.e. they have no offsprings. Mostly they suffer a violent death. It is very seldom that an animal dies of old age. It may happen to an elephant, or other animals with little predators.

Most of the humans often hold contradictory beliefs. On one hand, they see themselves as the "Pride of Creation" – a species of exceptional value and importance. On the other hand, people owe their very existence to evolution – a process driven by competition, suffering, and death. Evolution's engine is the elimination of those less fit to survive – including the death of those who carry 'unsuccessful' genetic material.

V. THE GLUT SOCIETY

In recent decades, several books have warned about the dangers of climate change and related environmental problems. I'd like to mention a few of them: the *Club of Rome*'s "The Limits to Growth" (1972) [3], *Rachel Carson*'s "Silent Spring" [4] (1962), which addresses the problems with the insecticide DDT, or "The Doomsday Book" by the British *Gordon Rattray Taylor* [5] (1970). Even before these well-known works the German author *Anton Metternich* wrote "Die Wüste droht" (The desert threatens) [6]. The book, published in 1947, warns of the possible spread of deserts in the future. Metternich wrote the foreword in 1944, and interestingly, there are only vague references to World War II – perhaps suggesting that, for him, the war was not the most significant global crisis. The book, however, was not successful. In those post– war years, the Germans had other concerns than the looming threat through climate change.

Today, we see a stark divide between wealthy countries like those in Europe, and many poorer countries around the world. I strongly believe that the prosperity of some nations depends on the poverty of others. Here in Germany, many goods are produced, but I doubt that this economic advantage can last 'indefinitely'. This situation will continue 100 or 200 years, but in the long run production takes its toll on the environment – particularly through agriculture, which slowly but surely removes the soil by the wind.

In my society, I am classified as to be 'at risk of poverty'. But I think that this is nonsense. Actually, I enjoy a lifestyle that 1000 years ago would have been almost unimaginable. For instance, every day I use warm water. Some people dream of an 'unconditional basic income', but this would be impossible due to the high costs. I believe firmly that if 'many' people have access to these comforts, this would ultimately destroy the environment.

People's desire for a comfortable life drives their pursuit of money, which in our society represents the key to comfort. Yet people often overlook the fact that money has no intrinsic value. Its worth comes entirely from a country's economic strength. When you have $ 20, you are not thinking of the physical bills – you're thinking what you can buy with that $ 20.

Germany's experience with hyperinflation around 1920 illustrates this well. When people lost faith in the currency, the money itself lost all value. Everybody was a millionaire, yet even with a million mark you couldn't buy a loaf of bread. I still own a postage stamp from that era with the face value of "10 Millionen".

Our system, capitalism, does offer some advantages such as personal freedom and social security. However, these benefits are not guaranteed; they are fortunate side effects rather than essential features of the system. History shows us that capitalism's alternatives – like communism, developed by the German thinker Karl Marx, has often failed even more dramatically.

Finally, I want to emphasize that these arguments reflect my personal opinions and subjective views. They are not presented as absolute truths – merely my perspective on the world as I see it.

ACKNOWLEDGEMENT

I thank Gavin Crosby for information, and as well as Lydia Ramachandran for a careful reading, and Oksana Fidan and David Searle for support.

REFERENCES

1. Der schöpferische Impuls Josef H. Reichholf (1992).
2. Das geheime Leben der Bäume Peter Wohlleben (2015).
3. The Limits to Growth Club of Rome (1972).
4. Silent Spring Rachel Carson (1962).
5. The Doomsday Book Gordon Rattray Taylor (1970).
6. Die Wüste droht Anton Metternich (1947).

Performance Assessment of Sugar Beet (*Beta vulgaris* L.) for Root and Yield Characters in Humid Tropics

PJ Arya, S. Sarad & T. Beena

Kerala Agricultural University

ABSTRACT

A study was conducted to assess the performance of sugar beet in humid tropical regions and to identify varieties/ hybrids, suitable to tropical conditions. The experimental material consisted of 30 sugar beet genotypes, including twenty-two varieties and eight hybrids. The experiment was laid out in RBD with three replications. Analysis of variance revealed significant differences among the twenty-two varieties and the eight hybrids for all the characters studied. Madhur recorded the highest root length of 7.43 cm among varieties and Red Star (Sakura) (7.41 cm) among hybrids. The highest root diameter of 5.33 cm was also recorded by Madhur and Ruby Queen (Tokita) (5.25 cm), Detroit Dark Red (5.16 cm) and Mahyco Lal II (5.15 cm) were statistically on par with it. The hybrid Red Star (Sakura) recorded the highest root diameter of 5.50 cm, which was on par with Ragini (5.32 cm). Madhur, among varieties and Red Star (Sakura), among hybrids recorded the highest root length (7.43 cm, 7.41 cm), root diameter (5.33 cm, 5.50 cm), root weight (118.05 g, 91.27 g), root: shoot ratio (4.42, 3.61) and yield per plot (5.68 kg, 4.27 kg), respectively. The varieties, Madhur, Tetra and Ruby Queen (Tokita) were early with a crop duration of 96 days, while the hybrids, Red Star (Sakura), Red Horse and RK 777 were early with a crop duration of 98 days. Madhur and Red Star (Sakura) were adjudged as the best performing variety and hybrid respectively, suitable for growing under humid tropical conditions..

Keywords: sugar beet, tropical varieties, tropical hybrids, mean performance, root yield.

Classification: LCC Code: QA351

Language: English

Great Britain Journals Press

LJP Copyright ID: 925674
Print ISSN: 2631-8490
Online ISSN: 2631-8504

London Journal of Research in Science: Natural & Formal

Volume 25 | Issue 7 | Compilation 1.0

Performance Assessment of Sugar Beet (*Beta vulgaris* L.) for Root and Yield Characters in Humid Tropics

PJ Arya, S. Sarada[α] & T. Beena[σ]

ABSTRACT

A study was conducted to assess the performance of sugar beet in humid tropical regions and to identify varieties/ hybrids, suitable to tropical conditions. The experimental material consisted of 30 sugar beet genotypes, including twenty-two varieties and eight hybrids. The experiment was laid out in RBD with three replications. Analysis of variance revealed significant differences among the twenty-two varieties and the eight hybrids for all the characters studied. Madhur recorded the highest root length of 7.43 cm among varieties and Red Star (Sakura) (7.41 cm) among hybrids. The highest root diameter of 5.33 cm was also recorded by Madhur and Ruby Queen (Tokita) (5.25 cm), Detroit Dark Red (5.16 cm) and Mahyco Lal II (5.15 cm) were statistically on par with it. The hybrid Red Star (Sakura) recorded the highest root diameter of 5.50 cm, which was on par with Ragini (5.32 cm). Madhur, among varieties and Red Star (Sakura), among hybrids recorded the highest root length (7.43 cm, 7.41 cm), root diameter (5.33 cm, 5.50 cm), root weight (118.05 g, 91.27 g), root: shoot ratio (4.42, 3.61) and yield per plot (5.68 kg, 4.27 kg), respectively. The varieties, Madhur, Tetra and Ruby Queen (Tokita) were early with a crop duration of 96 days, while the hybrids, Red Star (Sakura), Red Horse and RK 777 were early with a crop duration of 98 days. Madhur and Red Star (Sakura) were adjudged as the best performing variety and hybrid respectively, suitable for growing under humid tropical conditions.

Keywords: sugar beet, tropical varieties, tropical hybrids, mean performance, root yield.

Author α σ: Department of Vegetable Science, College of Agriculture, Vellayani, Kerala Agricultural University, Thiruvananthapuram, PIN- 695 522, Kerala, India.

London Journal of Research in Science: Natural & Formal

I. INTRODUCTION

Sugar beet (*Beta vulgaris* L.), known by various names, *viz.* beet, red beet, table beet, garden beet, *etc.*, is a cool season root vegetable crop, belonging to the family Amaranthaceae. It is indigenous to Southern Europe (Campbell, 1979). During 8000 B.C., beet cultivation began in Mesopotamia, later in Asia minor and spread to Meditteranean region (Biancardi *et al.,* 2012). Sugar beet is a highly productive, popular root vegetable, grown mainly for its fleshy, enlarged roots, with variable shapes-globular, cylindrical, top like and flattened. It is a rich source of carbohydrate (9.56 g 100 g^{-1}), protein (1.61g $100g^{-1}$), dietary fibre (2.8 g $100g^{-1}$), vitamin A (33 IU $100g^{-1}$), vitamin C (4.9 mg $100g^{-1}$), folate (109 µg $100g^{-1}$) and minerals *viz.*, potassium (325 mg $100g^{-1}$), sodium (78 mg $100g^{-1}$), phosphate (40 mg $100g^{-1}$), calcium (16 mg $100g^{-1}$), zinc (0.35 mg $100g^{-1}$) and iron (0.80 mg $100g^{-1}$) (Chawla *et al.*, 2016). The main nitrogen pigment present in sugar beet known as betalains comprising of red coloured β-cyanin and yellow coloured β- xanthin have antioxidant property (Singh and Hathan, 2014), anti-inflammatory effect (Neha *et al.*, 2018), hepatoprotective and anti-cancer properties (Chhikara *et al.*, 2018).

Sugar beet is generally grown during the winter season since good quality tubers, rich in sugar with intense red colour, are obtained during cool weather, when temperatures vary between 18.3 °C and 21.1 °C (Nath *et al.*, 1987). Cultivation of sugar beet has not become popular in tropical regions, while the demand is increasing due to its nutritional and health benefits. Sugar beet is having minimum cost of cultivation and gives bumper production with higher market value, but the crop remains neglected. The major reason is lack of awareness about scientific production as well as production technology under varying climatic conditions (Gaharwar *et al.*, 2017). Identification of a variety/ hybrid, suited to the growing condition is most important for successful commercial cultivation. Hence the present investigation was taken up with the objective to assess the performance of sugar beet in humid tropical regions and to identify varieties/ hybrids, suitable to tropical conditions.

II. MATERIALS AND METHODS

2.1 Experimental site

The present investigation was carried out at the Department of Vegetable Science, College of Agriculture, Vellayani, Kerala, India during 2019-'20. The experimental field was located at about 8.5° North latitude and 76.9° East longitude, with an average altitude of 29.00 m above mean sea level. The area enjoys a warm humid tropical climate and the average rainfall during the cropping season was 3.62 mm. The average minimum and maximum temperatures were 23.83°C and 32.36°C respectively and the average relative humidity varied from 57.90% to 106.00%. The principal soil type of the site was red loam belonging to the Vellayani series, texturally classified as sandy clay loam.

2.2 Plant materials

Thirty genotypes of sugar beet, consisting of 22 varieties and 8 hybrids were collected from public and private sectors. The details of the sugar beet varieties and hybrids used for the experiment are given in Table 1 and Table 2 respectively.

2.3 Experimental design and layout

The experiment was laid out in a Randomized Complete Block Design (RBD) with three replications. The seeds were sown at a spacing of 45 cm x 20 cm with 50 plants per plot and a plot size of 4.5 m^2. The season of cultivation was October to February.

2.4 Cultivation

Seeds of 22 varieties and 8 hybrids of sugar beet were sown in protrays filled with growing media composed of coir pith and vermicompost in the ratio 1:1 (Plate 1). Twenty-one days old seedlings were transplanted into the main field at a spacing of 45 cm x 20 cm in raised beds. Farmyard manure was applied @ 20 t ha^{-1} as basal. N, P and K were applied @ 37.50 t ha^{-1} as basal. Remaining N @ 37.50 t ha^{-1} was applied as top dressing, when the plant started growing vigorously. Weeding was done at regular intervals. Intercultural operations such as shallow hoeing and earthing up was done to facilitate root growth. General view of the experimental field is shown in Plate 2.

2.5 Observations Recorded

The observations were recorded from five randomly selected plants from each plot in each replication for the characters *viz.* root shape (IPGRI, 1995), root length, root diameter, root weight, root: shoot ratio, yield per plot and crop duration.

2.6 Statistical Analysis

Statistical analysis was carried out for varieties and hybrids individually using MS-Excel, WASP 2.0, OPSTAT and WINDOSTAT. For estimation of different statistical parameters, following procedure and formulae were adopted:

Analysis of Variance

The mean values observed for root and yield characters of fifteen plants (5 plants per plot per replication) were recorded and tabulated. The observations recorded were subjected to ANOVA (Panse and Sukhatme, 1985) for comparison among various treatments and to estimate variance components.

ANOVA for each character

Sources of variation	Degrees of freedom	Mean sum of squares	F ratio
Replication	r-1	MSR	MSR/MSE
Treatment	t-1	MST	MST/MSE
Error	(r-1) (t-1)	MSE	
Total	rt-1		

Where,

r = number of replications
t = number of treatments
MSR= mean sum of replication
MST= mean sum of treatments
MSE= mean sum of error

$$Critical\ difference\ (CD) = t\alpha \sqrt{\frac{2MSE}{r}}$$

Where, t = Student's 't' table value at error degrees of freedom at α level of significance.

III. RESULTS AND DISCUSSION

Tables 3 and Table 4 present the mean values for root and yield characters of sugar beet varieties and hybrids respectively. Significant differences was observed among the varieties and among hybrids for root and yield characters such as root shape, root length, root diameter, root weight, root: shoot ratio, yield per plot and crop duration.

3.1 Root shape

Among the 22 varieties, fifteen *viz.*, Madhur, Detroit Dark Red, Ruby Queen (Nisco), Tetra, Ruby Queen (Tokita), Mahyco Lal II, K 5340, K 5343, Red Ruby, Red star (Condor), K 5341, Ruby Queen (Suvarna), Rachna, Ruby Queen (Sulthan) and Indam Ruby Queen exhibited circular shaped root, five *viz.*, Lallan, Pure seeds, BV 20, BV 21 and Ruby Queen (Pradham Seeds) exhibited narrow elliptic shaped roots and two *viz.*, Crimson Globe and Royal displayed broad elliptic shaped roots. Four hybrids *viz.*, F_1 Kingdom, Red Star (Sakura), RK 777, and Ragini exhibited broad elliptic shaped roots while F_1 Kestral, Red Horse, Remo and Red Bull displayed narrow elliptic shaped roots. Ruboczki *et al.* (2015) reported sufficient variation among genotypes for root shape in sugar beet. Most of the varieties were circular in shape, which is favoured by not only the processing industry, but also the fresh market. Baranski *et al.* (2001) studied the diversity in a collection of 40 accessions of garden beet and reported circular root shape as the most common.

3.2 Root length

Among varieties, the longest root of 7.43 cm was recorded by Madhur, while the shortest by Lallan (3.03 cm). Among hybrids, the longest root of 7.41 cm was recorded by Red Star (Sakura) while the shortest by Red Bull (3.43 cm). These results are in consonance with Patel *et al.* (2015) and Coutinho *et al.* (2018) that considerable differences occur among sugar beet cultivars for length of root.

3.3 Root Diameter

The highest root diameter was observed for Madhur (5.33) and Ruby Queen (Tokita) (5.25 cm), Detroit Dark Red (5.16 cm) and Mahyco Lal II (5.15 cm) were statistically on par with it. The lowest diameter of 2.77 cm was recorded in Lallan. The mean root diameter was 4.33 cm. The average root diameter of hybrids ranged from 3.02 cm to 5.50 cm, with a mean of 4.36 cm. The highest root diameter was recorded in Red Star (Sakura) (5.50 cm), which was on par with Ragini (5.32 cm). The lowest root diameter of 3.02 cm was recorded in Red Bull. Varietal variation for root diameter in sugar beet was earlier reported by Coutinho *et al.* (2018). Root diameter has a positive effect on root yield, which is in line with the findings of Dongarwar *et al.* (2018) in radish. Yasaminshirazi *et al.* (2020) reported that roots with a diameter of 5 cm to 13 cm are considered for determining marketable yield in sugar beet. According to Baranski *et al.* (2001), market roots in garden beet defined roots with 4 to 8 cm diameter. The rapid increase in root width in radish is attributed by Alam *et al.* (2010) to translocation of more photosynthates from leaves to root.

3.4 Root Weight

Root weight ranged from 20.52 g to 118.05 g for varieties, with an overall mean of 57.63 g. The highest root weight was observed in Madhur (118.05 g), while the lowest in Lallan (20.52 g) (Fig. 2). Among the hybrids, the root weight ranged from 29.70 g to 91.27g, with a mean of 62.80 g. The highest root weight was recorded in Red Star (Sakura) (91.27 g) and lowest in Red Bull (29.70 g) (Fig. 4). Root weight is a primary character to be considered in any crop improvement programme, as it directly contributes towards yield. Yield is influenced by growth and the potential of a cultivar or hybrid. Among the varieties and hybrids, the genotype with the longest root and the highest root diameter recorded the highest root weight also. This is in conformity with the results of Yasaminshirazi *et al.* (2020). Maximum root weight might be because of the genetic capacity of the genotype to make available higher assimilates for root development.

Cultivar differences in root length, root diameter and root weight are in line with the results obtained by Ijoyah *et al.* (2008), Patel *et al.* (2015) and Sharma (2013) in sugar beet; Poleshi *et al.* (2017) in carrot; Alam *et al.* (2010), Poudel *et al.* (2018) and Dongarwar *et al.* (2018) in radish. This could be attributed to the difference in genetic makeup of the different varieties and ecological conditions. In the case of hybrids, higher root weight per plant was due to more number of leaves for photosynthesis and efficient utilization of these photosynthates, might have enhanced the better root length, root width and root yield per plant. This is in agreement with the findings of Patel *et al.* (2015) in sugar beet and Alam *et al.* (2010) in radish.

3.5 Root: Shoot Ratio (Weight Basis)

The highest root: shoot ratio was recorded by Madhur (4.42) and the lowest by BV 21 (0.77). Among the hybrids, the highest root: shoot ratio of 3.61 was recorded by Red Star (Sakura) and the lowest by Red Bull (1.54). Similar varietal variation in root: shoot ratio was reported by Sharma (2013) in sugar beet.

3.6 Yield per plot

The highest yield per plot of 5.68 kg was recorded by Madhur and the lowest by Lallan (1.03 kg) (Fig. 1). The mean yield per plot was 2.14 kg. The average yield per plot of hybrids ranged from 1.67 kg to 4.27 kg, with a mean of 3.04 kg. The highest yield per plot was recorded by Red Star (Sakura) (4.27 kg) and the lowest by Red Bull (1.67 kg) (Fig. 2). According to Sharma (2013), root yield per plot is one of the most desirable traits with the highest consideration in any sugar beet breeding programme. Significant variation in yield per plot might be due to the difference in root length, root diameter and root weight, which are the important components of yield. These findings are in line with those of Sharma (2013) in sugar beet.

3.7 Crop Duration

Crop duration of varieties ranged from 96 days to 130 days. Early crop of 96 days duration was observed in Madhur, Tetra and Ruby Queen (Tokita). The varieties, Ruby Queen (Pradham Seeds), BV 20, BV 21, Pure Seeds, Ruby Queen (Sulthan), Rachna and Lallan were late to harvest (130 days). Among the hybrids, Red Star (Sakura), Red Horse and RK 777 recorded early crop (98 days) and Red Bull, late (130 days). Difference in crop duration may be due to the genetic composition of the genotypes. Ijoyah *et al.* (2008) linked the time of maturity to the genetic control of the sugar beet varieties, thus the difference in the length of time taken to remain at the vegetative phase before roots are initiated and become matured.

IV. CONCLUSION

Based on the mean performance of the varieties and the hybrids for root and yield characters, Madhur, among varieties and Red Star (Sakura), among hybrids recorded the highest root length (7.43 cm, 7.41 cm), root diameter (5.33 cm, 5.50 cm), root weight (118.05 g, 91.27 g), root: shoot ratio (4.42, 3.61) and yield per plot (5.68 kg, 4.27 kg), respectively (Plates 3 and 4). Hence Madhur and Red Star (Sakura) were adjudged as the best performing variety and hybrid respectively, suitable for growing under humid tropical conditions.

REFERENCES

1. Alam, M.K., A.M. Farooque, M. Nuruzzaman and A.F.M.J. Uddin. (2010). Effect of sowing time on growth and yield of three radish (*Raphanus sativus* L.) varieties. Bangladesh Res. Pub. J. 3(3): 998-1006.
2. Baranski, R., D. Grzebelus, and L. Frese. (2001). Estimation of genetic diversity in a collection of the garden beet group. Euphytica 122(1): 19-29.
3. Biancardi, E., L.W. Panella and R.T. Lewellen. (2012). Beta maritime: The origin of beets, Springer, New York, USA. 7p.
4. Campbell, G.K.G. (1979). Sugar beet in evolution of crop plants, (Simmonds, N.W., Ed.). Longmans, N.Y. Green, London. pp.130.
5. Chawla, H., M. Parle, K. Sharma and M. Yadav. (2016). Beetroot: A health promoting functional food. Inventi. Rapid: Nutraceuticals, 1(1):0976-3872.
6. Chhikara, N., K. Kushwaha, P. Sharma, Y. Gat and A. Panghal. (2018). Bioactive compounds of beetroot and utilization in food processing industry: a critical review. Food Chem. 272:192-200.
7. Coutinho, P.W., M.M. Echer, P.S. Oliveira, G.M. Dalastra, D.A. Cadorin, and J. Vanelli. (2018). Productivity and qualitative characteristics of varieties of beets. J. Agri. Sci. 10(6): 327-333.
8. Dongarwar, L.N., R. Sumedh, S.R. Kashiwar, S.M. Ghawade, and U.R. Dongarwar. (2018). Varietal Performance of Radish (*Raphanus sativus* L.) Varieties in Black Soils of Vidharbha – Maharashtra. Int. J. Curr. Microbiol. App. Sci. 7(1): 491-501.

9. Gaharwar, A.M., J.D. Ughade, and N.V. Patil. (2017). Growth and productivity of sugar beet (*Beta vulgaris* L.) with monetary returns as affected by different spacings. Asian J. Bio Sci. 12(2): 189-193.
10. Ijoyah, M.O., V.L. Sophie, and H. Rakotomavo. (2008). Yield performance of four beetroot (*Beta vulgaris* L.) varieties compared with the local variety under open field conditions in Seychelles. Agro. Sci. 7(2): 139-142.
11. IPGRI [International Plant Genetic Recourses Institute]. (1995). Descriptors for Beta (*Beta* spp.). Rome, Italy, 37p.
12. Nath, P., S. Velayudhan and D.P. Singh. (1987). Vegetables for the tropical region. ICAR, New Delhi, pp. 60-61.
13. Neha, P., J. Sk, J. Nk and J. Hk, (2018). Chemical and functional properties of Beetroot (*Beta vulgaris* L.) for product development: A review. Int. J. Chem. Stud. 6:3190-3194.
14. Panse, V.G. and P.V. Sukhatme. (1985). *Statistical Methods for Agricultural Workers* (4th Ed.). Indian Council of Agricultural Research, New Delhi, 347p.
15. Patel, H.T., M.K. Sharma and L.R. Varma. (2015). Effect of planting date and spacing on growth, yield and quality of sugar beet (*Beta vulgaris* L.) cultivars under North Gujarat climatic conditions. Int. J. Agric. Sci. Res. 5(4): 119-125.
16. Poleshi, C.A., S. Cholin, D.S. Manikanta and D.S. Ambika. (2017). Genetic variability for root traits in carrot (*Daucus carota* L.) evaluated under tropical condition. Ann. Hortic. 10(2): 224-227.
17. Poudel, K., S. Karki, M.K. Sah and J.L. Mandal. (2018). Evaluation of radish (*Raphanus sativus* L.) genotypes in Eastern mid-hills condition of Nepal. World News Nat. Sci. 19: 155-159.
18. Ruboczki, T., V. Raczko and M.T. Hajos. (2015). Evaluation of morphological parameters and bioactive compounds in different varieties of beetroot (*Beta vulgaris* L. ssp. *esculenta* GURKE var. *rubra* L.). Int. J. Hortic. Sci. 21(4): 31-35.
19. Sharma, M. (2013). Studies on genetic evaluation of sugar beet *(Beta vulgaris* L.*)*. M.Sc. (Hortic.) thesis, Dr. Yashwant Singh Parmar University of Horticulture and Forestry, Nauni, Solan, 76p.
20. Singh, B. and B.S. Hathan. (2014). Chemical composition, functional properties and processing of beetroot-a review. Int. J. Sci. Eng. Res. 5 (1): 679-684.
21. Yasaminshirazi, K., J. Hartung, R. Groenen, T. Heinze, M. Fleck, S. Zikeli and S. Graeff-Hoenninger. (2020). Agronomic performance of different open-pollinated beetroot genotypes grown under organic farming conditions. Agron. 10(6): 812.

Table 1: Details of sugar beet varieties used for the study

Treatment number	Accession number	Name of variety	Source
T1	BV 1	Madhur	Namdhari Seeds, Bengaluru
T2	BV 2	Detroit Dark Red	IARI, New Delhi
T3	BV 3	Crimson Globe	IARI, New Delhi
T4	BV 4	Ruby Queen (Nisco)	NISCO, Bengaluru
T5	BV 5	Tetra	Clause, Bengaluru
T6	BV 6	Ruby Queen (Tokita)	Tokita Seeds, Tamil Nadu
T7	BV 7	Mahyco lal II	Mahyco, Maharashtra
T8	BV 8	Royal	Bengaluru
T9	BV 9	K 5340	Kalash Seeds, Jalna, Maharashtra
T10	BV10	K 5343	Kalash Seeds, Jalna, Maharashtra
T11	BV 11	Red Ruby	Doctors Seeds, Bengaluru

T12	BV 12	Red Star (Condor)	Condor Seeds, Bengaluru
T13	BV 13	K5341	Kalash Seeds, Jalna, Maharashtra
T14	BV 14	Ruby Queen (Suvarna)	Suvarna, Bengaluru
T15	BV 15	Lallan	NISCO Seeds, Bengaluru
T16	BV 16	Rachna	Shine Seeds, Bangaluru
T17	BV 17	Ruby Queen (Sulthan)	Sulthan, Bengaluru
T18	BV 18	Indam Ruby Queen	IAHS, Bengaluru
T19	BV 19	Pure Seeds	Pure Seeds, Karnataka
T20	BV 20	BV 20	Jaiva Samrthi Kudumbasree Unit, Thodiyoor, Karunagapally
T21	BV 21	B V 21	Jaiva Samrthi Kudumbasree Unit, Thodiyoor, Karunagapally
T22	BV 22	Ruby Queen (Pradham Seeds)	Pradham Seeds, Karnataka

Table 2: Details of sugar beet hybrids used for the study

Treatment number	Accession number	Name of hybrid	Source
H1	BV 23	F_1 Kingdom	Sakura, Bengaluru
H2	BV 24	F_1 Kestral	Sakura, Bengaluru
H3	BV 25	Red Star (Sakura)	Sakura, Bengaluru
H4	BV 26	Red Horse	R K seeds, New Delhi
H5	BV 27	RK777	R K seeds, New Delhi
H6	BV 28	Remo	Ashoka seeds, Bengaluru
H7	BV 29	Red Bull	Sakura, Bengaluru
H8	BV 30	Ragini	Netra seeds, Begaluru

Table 3: Mean performance of sugar beet varieties for root and yield characters

Treatments		Root shape	Root length (cm)-	Root diameter (cm)	Root weight (g)	Root: shoot Ratio	Yield per plot (kg)	Crop duration (Days)
V1	Madhur	Circular	7.43	5.33	118.05	4.42	5.68	96
V2	Detroit Dark Red	Circular	6.19	5.16	80.93	3.66	4.04	98
V3	Crimson Globe	Broad elliptic	6.03	4.30	62.33	1.98	3.12	110
V4	Ruby Queen (Nisco)	Circular	5.54	4.27	56.38	2.14	2.82	110
V5	Tetra	Circular	5.55	4.85	63.82	1.22	3.19	96
V6	Ruby Queen (Tokita)	Circular	6.21	5.25	85.65	3.16	4.78	96
V7	Mahyco Lal II	Circular	6.07	5.15	80.39	2.27	4.02	98

V8	Royal	Broad elliptic	6.05	5.11	77.13	3.23	3.86	98
V9	K 5340	Circular	5.30	4.28	48.58	1.99	2.43	110
V10	K 5343	Circular	5.32	4.60	61.11	2.41	3.06	98
V11	Red Ruby	Circular	4.97	3.56	55.11	2.41	2.76	110
V12	Red Star (Condor)	Circular	4.82	3.68	53.82	2.07	2.68	110
V13	K5341	Circular	4.78	4.89	56.78	2.31	2.81	110
V14	Ruby Queen (Suvarna)	Circular	5.75	4.43	61.17	2.42	3.09	110
V15	Lallan	Narrow elliptic	3.03	2.77	20.52	0.94	1.03	130
V16	Rachna	Circular	5.23	4.48	58.49	2.34	2.93	130
V17	Ruby Queen (Sulthan)	Circular	5.10	4.63	59.25	2.15	2.97	130
V18	Indam Ruby Queen	Circular	6.10	4.93	78.46	2.95	3.85	110
V19	Pure Seeds	Narrow elliptic	3.55	4.72	22.83	0.93	1.14	130
V20	BV 20	Narrow elliptic	4.21	3.33	23.51	0.90	1.20	130
V21	BV 21	Narrow elliptic	4.20	2.85	21.56	0.77	1.07	130
V22	Ruby Queen (Pradham Seeds)	Narrow elliptic	4.76	2.80	22.08	0.80	1.08	130
MEAN			5.28	4.33	57.63	2.16	2.14	
SEm(±)			0.13	0.06	0.83	0.09	0.08	
CD (0.05)			0.37	0.18	1.67	0.25	0.24	

Table 4: Mean performance of sugar beet hybrids for root and yield characters

Treatments		Root shape	Root length (cm)	Root diameter (cm)	Root weight (g)	Root: shoot ratio	Yield per plot (kg)	Crop duration (Days)
H1	F_1 Kingdom	Broad elliptic	6.03	4.50	69.21	2.69	3.33	110
H2	F_1 Kestral	Narrow elliptic	4.74	3.76	43.02	1.93	2.06	110
H3	Red Star (Sakura)	Broad elliptic	7.41	5.50	91.27	3.61	4.27	98
H4	Red Horse	Narrow elliptic	6.50	4.88	77.23	3.27	3.82	98
H5	RK777	Broad elliptic	5.39	4.17	61.38	1.98	3.00	98
H6	Remo	Narrow elliptic	4.08	3.74	42.23	1.72	2.05	110
H7	Red Bull	Narrow elliptic	3.43	3.02	29.70	1.54	1.67	130

H8	Ragini	Broad elliptic	7.11	5.32	84.23	3.29	4.09	110
MEAN			5.59	4.36	62.80	2.05	3.04	
SEm(±)			0.06	0.1	0.58	0.08	0.06	
CD (0.05)			0.18	0.31	1.77	0.24	0.177	

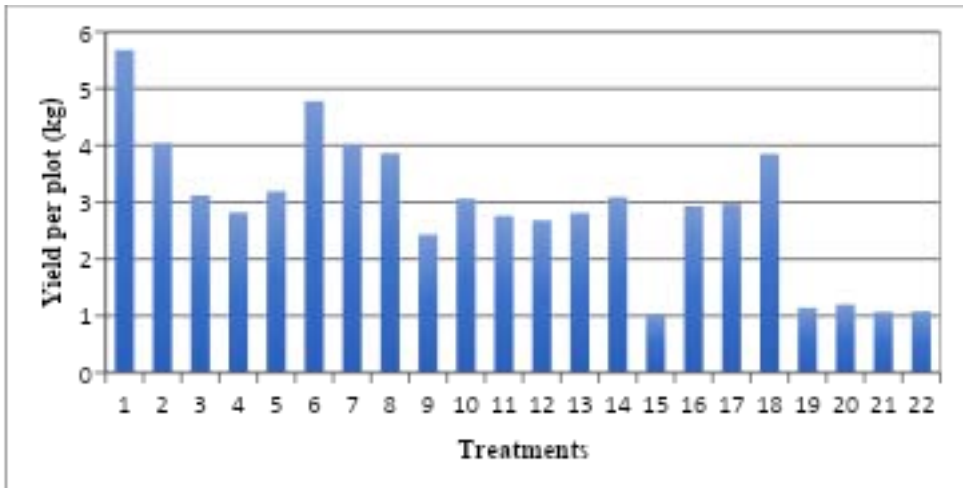

Fig. 1: Mean performance of sugar beet varieties for yield per plot(kg)

X axis: 1. Madhur 2. Detroit Dark Red 3. Crimson Globe 4. Ruby Queen (Nisco) 5. Tetra 6. Ruby Queen (Tokita) 7. Mahyco Lal II 8. Royal 9. K5340 10. K 5343 11. Red Ruby 12. Red Star (Condor) 13. K5341 14. Ruby Queen (Suvarna) 15. Lallan 16. Rachna 17. Ruby Queen (Sulthan) 18. Indam Ruby Queen 19. Pure Seeds 20. BV 20 21. BV 21 22. Ruby Queen (Pradham Seeds).

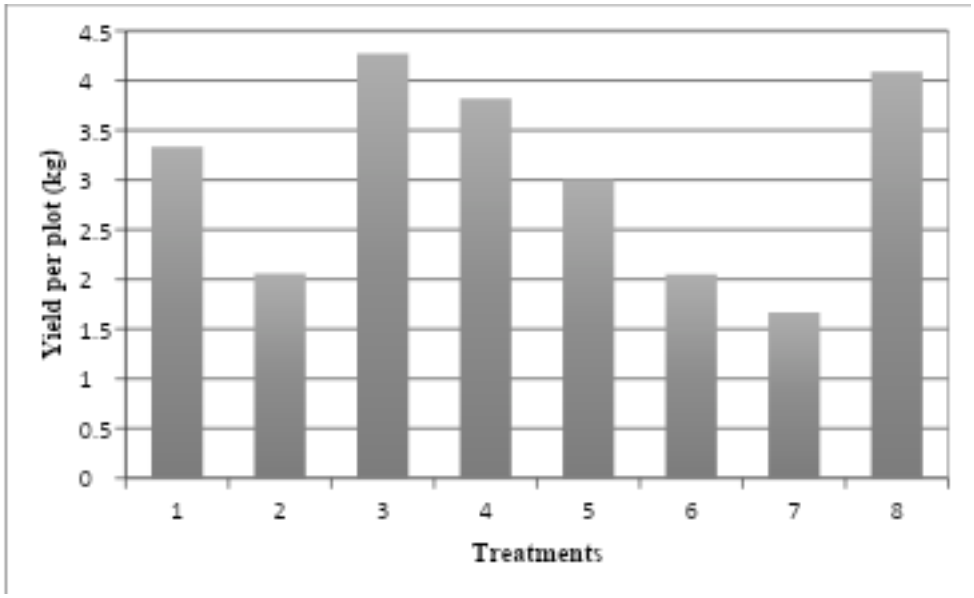

Fig 2: Mean performance of sugar beet hybrids for yield per plot (kg)

X axis: F1 Kingdom 2. F1 Kestral 3. Red Star (Sakura) 4. Red Horse 5. RK 777 6. Remo 7. Red Bull 8. Ragini

Plate 1: Seedlings in protrays

Plate 2: General view of experimental field

Plate 3: Best performing sugar beet variety- Madhur

This page is intentionally left blank

Influence of Bacau City's Anthropic Activities on the Heavy Metals Concentration Measured on Bistrita and Siret River Sides

Alexandra-Dana Chitimus, Florin-Marian Nedeff, Ion Sandu, Cristian Radu, Emilian Mosnegutu & Ioan Gabriel Sandu

Vasile Alecsandri University of Bacau

ABSTRACT

The main objective of the current research is to determine the content of heavy metals from the Bistrita and Siret River banks, respectively Siret River – in Bridge Holt area, Siret River – canal UHE and Siret River- downstream confluence Bistrita/Siret. The choice of sampling points took into consideration the areas where the pollution sources are located. Established maximum values were not exceeded in the case of mercury in the soil for all three sampling points Siret River – in Bridge Holt area, Siret River – canal UHE and Siret River- downstream confluence Bistrita/Siret. Exceeding values recorded in the sampling points Siret River – in Bridge Holt area, Siret River – canal UHE and Siret River- downstream confluence Bistrita/Siret (for cadmium, nickel and chrome) resulted from discharged residual waters, industrial platforms from Bacau city and the improper storage of municipal waste.

Keywords: heavy metals, soil, pollution, siret river sides.

Classification: LCC Code: TD878, GE160, QH545.M3

Language: English

Great Britain Journals Press

LJP Copyright ID: 925675
Print ISSN: 2631-8490
Online ISSN: 2631-8504

London Journal of Research in Science: Natural & Formal

Volume 25 | Issue 7 | Compilation 1.0

Influence of Bacau City's Anthropic Activities on the Heavy Metals Concentration Measured on Bistrita and Siret River Sides

Alexandra-Dana Chitimus[α], Florin-Marian Nedeff[σ] , Ion Sandu[ρ], Cristian Radu[ↀ], Emilian Mosnegutu[§] & Ioan Gabriel Sandu [χ]

ABSTRACT

The main objective of the current research is to determine the content of heavy metals from the Bistrita and Siret River banks, respectively Siret River – in Bridge Holt area, Siret River – canal UHE and Siret River- downstream confluence Bistrita/Siret. The choice of sampling points took into consideration the areas where the pollution sources are located. Established maximum values were not exceeded in the case of mercury in the soil for all three sampling points Siret River – in Bridge Holt area, Siret River – canal UHE and Siret River- downstream confluence Bistrita/Siret. Exceeding values recorded in the sampling points Siret River – in Bridge Holt area, Siret River – canal UHE and Siret River- downstream confluence Bistrita/Siret (for cadmium, nickel and chrome) resulted from discharged residual waters, industrial platforms from Bacau city and the improper storage of municipal waste.

Keywords: heavy metals, soil, pollution, siret river sides.

Author α σ §: Vasile Alecsandri University of Bacau, Faculty of Engineering, 157 Calea Marasesti, 600115, Bacau, Romania.
ρ: Alexandru Ioan Cuza University of Iasi, Arheo Invest Interdisciplinary Platform, Scientific Investigation Laboratory, 11 Carol I Blvd., 700506, Iasi, Romania.
ρ χ: Romanian Inventors Forum, 3 Sf. Petru Movila St., Bloc L11, III/3, 700089, Iasi, Romania.
ↀ: Romanian Waters - National Administration of Siret Basin, 1 Cuza Voda Str., 600274, Bacau, Romania.
χ: Gheorghe Asachi Technical University of Iasi, Materials Science and Engineering Faculty, 53A D. Mangeron Blvd., 700050, Iasi, Romania.

London Journal of Research in Science: Natural & Formal

I. INTRODUCTION

Naturally, heavy metals are held in the soil in relatively low concentrations but may occur in high concentrations with toxic potential, as a result of anthropogenic and especially uncontrolled activities. In this alternative, of their excess, heavy metals can cause disturbances in soil, plants and water and subsequently in the upper links of the food chain [1-11].

The pollution of the environment with heavy metals through human activities has caused their accumulation in surface waters, sediments and soil, especially in industrial areas [2, 5, 8, 12-19].

Heavy metal soil pollution has a cumulative character, which means that the pollutants accumulate slowly, being the result of permanent and long-term exposure of the soil to the action of these pollutants, without decomposing and without being able to remove them, whence and their permanent character. Once polluted, soils can only regenerate very hard and thus reduce their fertility [2, 5, 8, 19-41].

Research aimed to determine the influence of industrial activities carried out in Bacau city on the contents of heavy metals on the banks of Bistrita and Siret River. This influence was determined by analyzing the concentrations of heavy metals Siret River – in Bridge Holt area, Siret River – canal UHE and Siret River- downstream confluence Bistrita/Siret, in locations along the Bistrita and Siret River.

II. EXPERIMENTAL PART

For the selection of sampling points we had in view the areas where pollution sources are located. For every sampling section, sediments must be samples from representative places, so that we could have exact knowledge of the pollution sources as well as of the hydrological and and geomorphologic characteristics of the area. The sampling points must represent areas in which the sediment layer is thick and its granulosity is lower than 63µm, consisting of clay and slime [2].

Sections targeted for the sample-taking programme are presented in Figure 1. Sediments were sampled Siret River – Bridge Holt area (S1), Siret River – canal UHE (S2) and Siret River- downstream confluence Bistrita/Siret (S3), in locations along the Bistrita and Siret River, and experiments were conducted so as to test four heavy metals, namely Cd, Ni, Cr and Hg [2].

The significant punctiform pollution sources are from industrial or agricultural area.

Soil samples were taken for three levels [2]:
- minimum level: soil-water interface level of 0 cm;
- medium level: soil-water interface level of 50 cm, on the river bank;
- maximum level: soil-water interface level of 100 cm, on the river bank.

In Governmental Order no. 161 as of February 16 2006, entitled Elements and standards concerning the chemical quality of the alluvia – section 63 µm, Table 1 presents the established maximum concentration levels for heavy metals in the soil [42].

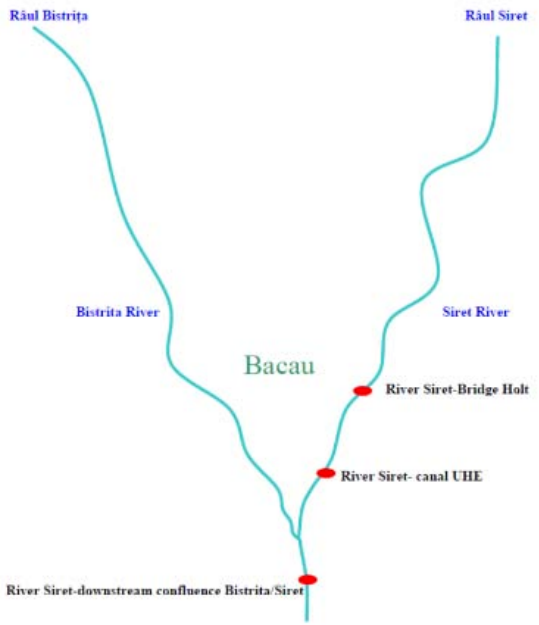

Fig. 1: The location of sampling points on the banks of Bistrita and Siret River, Siret River – Bridge Holt area, Siret River – canal UHE and Siret River- downstream confluence Bistrita/Siret.

Table 1: Elements And Standards Concerning The Chemical Quality Of The Alluvia [42].

Quality indicator	Unit of measure	Quality standard
Cadmium	[mg/kg d.m.]	0.8
Nickel		35
Chromium		100
Mercury		0.3

The cadmium, nickel, chromium and mercury soil content has been determined by using the atomic absorption spectrometer (AAS), ZEENIT AAS version (fig. 2) [2, 43].

Fig. 2: Atomic absorption spectrometer (AAS), Zeenit 700 version [43]

III. RESULTS AND DISCUSSIONS

Figure 3 represents the variations of cadmium concentration in the soil for sampling points Siret River – Bridge Holt area, Siret River – canal UHE and Siret River- downstream confluence Bistrita/Siret.

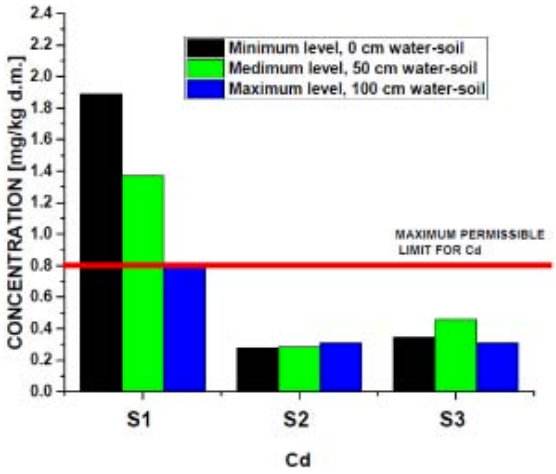

Fig. 3: Cadmium concentration in the soil for sampling points Siret River – Bridge Holt area, Siret River – canal UHE and Siret River- downstream confluence Bistrita/Siret

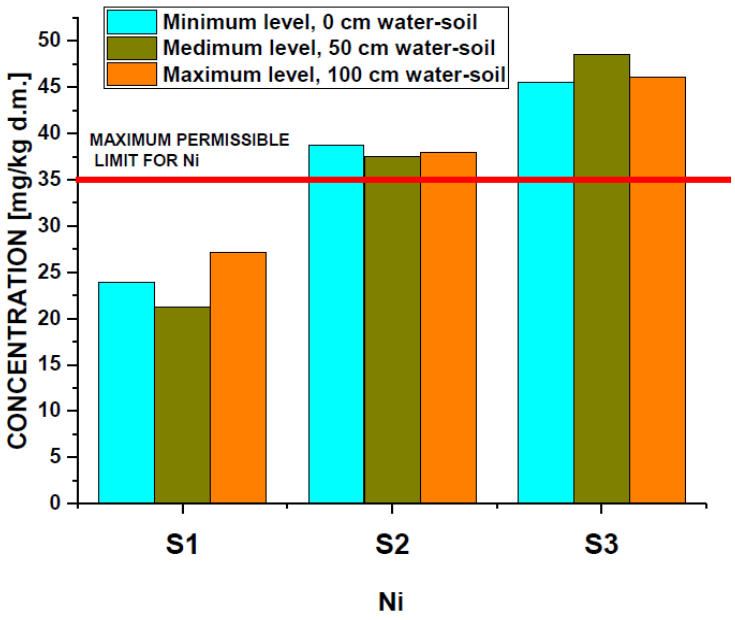

Fig. 4: Cadmium concentration in the soil for sampling points Siret River – Bridge olt area, Siret River – canal UHE and Siret River- downstream confluence Bistrita/Siret.

Nickel concentrations in the soil for sampling point Siret River – canal UHE exceeds established levels with 110.57 % for the soil-water interface level of 0 cm, and for the soil-water interface level of 50 cm the nickel concentration in the soil exceeded permitted limits with 107.22 %.

For a soil-water interface level of 100 cm the maximum established limit for nickel in the soil is exceeded with 107.57 %.

The established maximum level for nickel, in the soil is exceeded in sampling point Siret River-downstream confluence Bistrita/Siret for all three level so:

- minimum level water-soil interface (0 cm) with 130.22 %;
- medium level water-soil interface (50 cm) with 138.62 %;
- maximum level water-soil interface (100 cm) with 137.22 %.

The established maximum level for chromium (100 mg/kg d.m.), in the soil was not exceeded in sampling point Siret River – Bridge Holt (the maximal value obtained was for the minimum soil-water interface level of 0 cm – 57.11 mg/kg d.m., fig. 5).
The established maximum limit for chromium in the soil in the sampling point Siret River – canal UHE is exceeded with 154.2 % for the soil-water interface level of 0 cm.

For sampling point Siret River – canal UHE, the established maximum limit for chromium in exceeded with 133.4 % for the medium level soil-water interface and with 152.3 % for the maximal level soil-water interface.

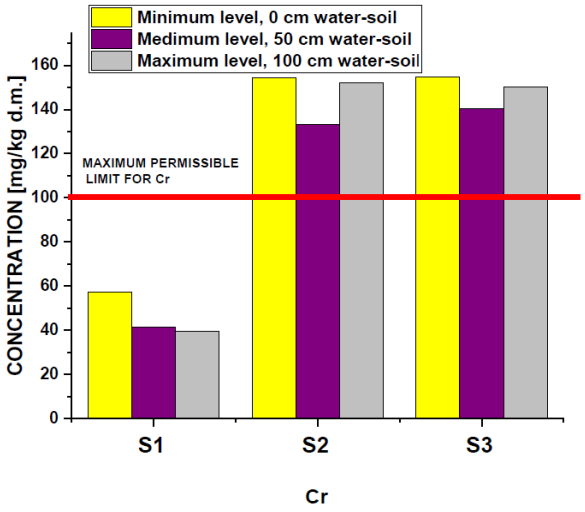

Fig. 5: Chromium concentration in the soil for sampling points Siret River – Bridge Holt area, Siret River – canal UHE and Siret River- downstream confluence Bistrita/Siret

The established maximum level for chromium, in the soil is exceeded in sampling point Siret River-downstream confluence Bistrita/Siret for all three level and the higher value was registered for the minimum level soil-water interface (154.7 mg/kg d.m.):

The established maximum level for mercury, in the soil is not exceeded in al three sampling points, so the value obtained was (fig. 6):

- Sampling point Siret River – Bridge Holt: 0.038÷0.076 mg/kg d.m.;
- Sampling point Siret River – canal UHE: 0.066÷0.11 mg/kg d.m.;
- Sampling point Siret River downstream confluence Bistrita/Siret: 0.07÷0.082 mg/kg d.m.

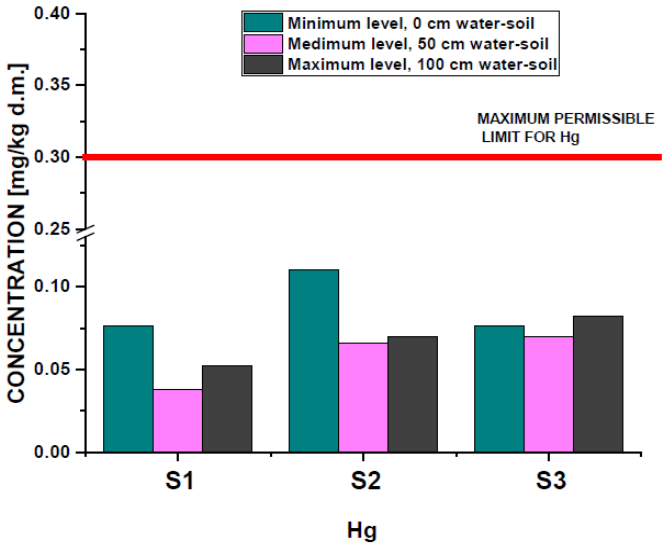

Fig. 6: Mercury concentration in the soil for sampling points Siret River – Bridge Holt area, Siret River – canal UHE and Siret River- downstream confluence Bistrita/Siret.

IV. CONCLUSIONS

The exceeding of limits of heavy metals (cadmium, nickel, chromium and mercury) in the soil is the result of urban wastewater discharged in Bistrita river by means of water treatment stations, industrial platforms form Bacau city, the inappropriate storage of municipal waste.

The higher value of concentration of heavy metal in the soil was registered for cadmium, for the sampling point Siret River – Bridge Holt, minimum level soil-water interface – 1.89 mg/kg d.m.

The established maximum limit for cadmium, nickel, chromium and mercury in the soil is not exceeded in the sampling points:

Siret River – canal UHE and Siret River- downstream confluence Bistrita/Siret-for all three levels (for cadmium); - Siret River – Bridge Holt - for all three levels (for nickel and chromium);

- The established maximum level for mercury in the soil is not exceeded in al three sampling points.

REFERENCES

1. OACA (IRIMIA), O., NEDEFF, V., PANAINTE-LEHADUS, M., TOMOZEI, C., Journal of Engineering Studies and Research, 22, no. 4, p. 54-61.
2. LUO, C.L., LIU, C.P., WANG, Y., XIANG, L., FANGBAI, L., GAN, Z., XIANGDONG, L., Journal of Hazardous Materials, 186, no. 1, 2011, p. 481.
3. RADU, C., CHITIMUS, A.D., TURCU, M., ARDELEANU, G., BELCIU M, Environmental Engineering and Management Journal, 13, no. 7, 2014, p. 1687.
4. ABDERRAHIM, G., European Journal of Scientific Research, 32, 2009, p. 58.
5. BELCIU, M.C., NEDEFF, V., CHITIMUS, A.D., BARSAN, N., RUSU, D., Journal of Engineering Studies and Research, 22, no. 1, 2016, p. 15.
6. RADU, C., NEDEFF, V., CHITIMUS, A.D., Journal of Engineering Studies and Research, 19, 2, 2013, p. 89. 9.AL-MOMANI, I.F., Jordan Journal of Chemistry, 4, 2009, p. 77.
7. CHITIMUS, A.D., NEDEFF, V., LAZAR, G., MACARESCU, B., MOSNEGUTU, E., Journal of Engineering Studies and Research, 17, no. 1, 2011, p. 13.
8. MUSCALU (PLESCAN), O.M., NEDEFF, V., CHITIMUS, A.D., PARTAL, E., MOSNEGUTU, E., RUSU, I.D., Rev.Chim. (Bucharest), 69, no. 11, 2018, p. 3106.
9. MUSCALU (PLESCAN), O.M., NEDEFF, V., CHITIMUS, A.D., PARTAL, E., BARSAN, N., RUSU, I.D, Rev.Chim. (Bucharest), 70, no. 2, 2019, p. 536-542.
10. CHARKRAVARTY, M., PATGIRI, A.D., Journal of Human Ecology, 27, 2009, p. 63.
11. CHITIMUS, A.D., BARSAN, N., NEDEFF, V., MOSNEGUTU, E., MUSCALU (PLESCAN), O., 17th International Multidisciplinary Scientific GeoConference SGEM 2017, 17, no. 51, 2017, p. 859.
12. CHITIMUS, A.D., NEDEFF, V., MOSNEGUTU, E., PANAINTE, M., Environmental Engineering and Management Journal, 11, 2012, p. 2161.
13. DRAGOVIĆ, S., MIHAILOVIĆ, NJUN, Y., SILU, M., JINGCHENG, Z., YONGWEI, S., FEI, L., Journal of International Medical Research, 46, no. 8, 2018, p.3374. 2.RADU, C., Studies and research on the ecological impact of residual soil pollution by heavy metals on tributaries' banks from the Siret hydrographic basin, phD Thesis, "Vasile Alecsandri" University of Bacau, Romania, 2015.
14. TIRT., GAJIĆ, B., Chemosphere, 74, 2008, p. 491.
15. JINTAO, L., CUICUI, C., XIULI, S., YULAN, H., ZHENHAI, L., International Journal of Electrochemical Science, 6, 2011, p. 5314. 18.MUSCALU (PLESCAN), O.M., NEDEFF, V., PARTAL, E., MOSNEGUTU, E., SANDU, I.G., SANDU, I., BARSAN, N., RUSU, D., Rev.Chim. (Bucharest), 70, no. 5, 2019, p.1726.

16. CHITIMUS, A.D., RADU, C., NEDEFF, V., MOSNEGUTU, E., BARSAN, N., Scientific Study & Research Chemistry & Chemical Engineering, Biotechnology, Food Industry, 17, no. 4, 2016, p. 381.
17. KIM, Y., KIM, B.K., KIM, K., Environmental Earth Sciences, 60, 2009, p. 943.
18. CHITIMUS, A.D., MOSNEGUTU, E., NICOLESCU, M.C., TURCU M., BELCIU, M.C., ARDELEANU, G., Environmental Engineering & Management Journal, 13, no. 7, 2014, p. 1581.
19. CHITIMUS, D., COCHIORCA, A., NEDEFF, V., MUSCALU, O., BARSAN, N., Proceeding of the International Multidisciplinary Scientific GeoConference Surveying Geology and Mining Ecology Management, SGEM, 18, 2018, p. 671.
20. CHITIMUS, A.D., NEDEFF, V., LAZAR, G., Journal of Engineering Studies and Research, 17, no. 4, 2011, p. 24. 24.MARTIN, L., Water Air Soil Pollution, 126, 2001, p. 363.
21. CHITIMUS, A.D., NEDEFF, V., SANDU, I., RADU, C., MOSNEGUTU, E., SANDU, I.G., BARSAN, B., Rev.Chim. (Bucharest), 70, no. 7, 2019, p. 2545.
22. CHITIMUS, A.D., NEDEFF, V., SANDU, I., RADU, C., MOSNEGUTU, E., SANDU, I.G., BARSAN, B., Rev.Chim. (Bucharest), 70, no. 8, 2019, p. 3058.
23. SENILA, M., LEVEI, E., MICLEAN, M., SENILA, L., STEFANESCU, L., MARGINEAN, S., OZUNU, A., ROMAN, C., Environmental Engineering and Management Journal, 10, 2011, p. 59.
24. 28.TOMOZEI, C., IRIMIA, O., VALENTIN, N., PANAINTE-LEHADUS, M., 17th International Multidisciplinary Scientific GeoConference SGEM 2017, Conference Proceedings, 51, no. 17, 2017, p. 635.
25. KESHAV, K. A., RAMA, M.K., Environmental Earth Sciences, 75, 2011, p. 411.
26. MOJGAN, Y., MAJID, A., KHOSHGOFTARMANESH, A.H., SOFFIANIAN, A.R., SCHULIN, R., Human and Ecological Risk Assessment: An International Journal, 18, no. 3, 2012, p. 547.
27. TURCU, M., BARSAN, N., IRIMIA, O., JOITA, I., BELCIU, M., Environmental Engineering and Management Journal, 13, no. 7, 2014, p. 1751.
28. BARSAN, N., NEDEFF, V., TEMEA, A, MOSNEGUTU, E., CHITIMUS, A. D., TOMOZEI, C., Chemistry Journal of Moldova, 12, no. 1, 2017, p. 61.
29. COCHIORCA, A., NEDEFF, V., BARSAN, N., MOSNEGUTU, E.F., PANAINTE-LEHADUS, M., TOMOZEI, C., Chemistry & Chemical Engineering, Biotechnology, Food Industry, 19, no. 4, 2018, p. 455.
30. FABIAN, F., NEDEFF, V., PANAINTE – LEHADUS, M., BARSAN, N., IRIMIA, O, RACOVITA, S., Journal of Engineering Studies and Research, 22, no. 3, 2016, p. 34.
31. TATARU, L., NEDEFF, V., BARSAN, N., MOSNEGUTU, E., PANAINTE LEHADUS, M., SANDU, I., CHITIMUS, D., Mat. Plast., 55, no. 4, 2018, p. 660.
32. TURCU, M., BARSAN, N., MOSNEGUTU, E., DASCALU, M., CHITIMUS, D., RADU, C., Environmental Engineering and Management Journal, 15, no. 3, 2016, p. 521.
33. TATARU, L., NEDEFF, V., BARSAN, N., SANDU, A.V., MOSNEGUTU, E., PANAINTE-LEHADUS, M., SANDU, I., Mat. Plast. 56, no. 1, 2019, p. 97.
34. MISAILA, L., NEDEFF, F.M., BARSAN, N., SANDU, I.G., GROSU, L., PATRICIU, O.I., GAVRILA, L., FINARU, A.L., Rev.Chim. (Bucharest), 70, no. 6, 2019, p. 2212.
35. SAMPAH, G.E., KOUAKOU, S.K., OI, M.J.M., NEDEFF, V., SANDU, A.V., BARSAN, N., SANDU, I., Rev.Chim. (Bucharest), 70, no. 7, 2019, p. 2579.
36. GOLDAN, E., NEDEFF, V., BARSAN, N., MOSNEGUTU, E., SANDU, A.V., PANAINTE, M., Rev.Chim. (Bucharest), 70, no. 3, 2019, p. 809.
37. GOLDAN, E., NEDEFF, V., SANDU, I., BARSAN, N., MOSNEGUTU, E., PANAINTE, M., Rev.Chim. (Bucharest), 70, no. 6, 2019, p. 2192.
38. *** Governmental Order no. 161 as of February 16, 2006, entitled Elements and standards concerning the chemical quality of the alluvial – section 63 μm.
39. ***Atomic absorption spectrometry (AAS) ZEEnit 700, Operating Manual, 2009.

This page is intentionally left blank

Modification of Kornevin Growth Powder for the purposes of Root Formation in Semi-Lignified Cuttings of Juníperus Sabína L.

Borovkov Vadim Valentinovich & Demchenko Gleb Aleksandrovich

ABSTRACT

In Russian nurseries, growth powders are widely used for rooting semi-lignified cuttings of coniferous crops. Due to the fact that the range of such powders is represented by preparations with only one concentration of the active substance (4 (indol-3-yl) butyric acid) - 5 g / l (0.5% IBA), a study was conducted on the possibility of diluting the preparations with talc and crushed charcoal using the Kornevin powder as an example. Semi-lignified cuttings of Juníperus sabína were used in the experiments; rooting was carried out under the conditions of installing low-pressure artificial fog with substrate heating. It was shown that the best option under the experimental conditions was the use of Kornevin-talc powder in a volume ratio of 1 to 1 to stimulate rooting. The rooting of the cuttings was 89.3%. Undiluted Kornevin had a phytotoxic effect, which caused a decrease in the survival rate from the values of the best option by 26%. The use of powders with a more significant dilution of Kornevin led to the appearance of signs of auxin deficiency in the stimulator. Thus, it was shown that for rooting cuttings of Juníperus sabína, powders with an IMC content of 0.25% are needed, which can be obtained by diluting Kornevin powder with talc or crushed charcoal. It was shown that when diluting growth powder, it is necessary to take into account that with the same degree of dilution (by powder volume), the hormonal properties of IMC decrease more intensively in options with crushed charcoal than talc.

Keywords: juníperus sabína, propagation, rooting, growth powders, auxins.

Classification: LCC Code: SB435.5, QK725

Language: English

Great Britain Journals Press

LJP Copyright ID: 925676
Print ISSN: 2631-8490
Online ISSN: 2631-8504

London Journal of Research in Science: Natural & Formal

Volume 25 | Issue 7 | Compilation 1.0

Modification of Kornevin Growth Powder for the purposes of Root Formation in Semi-Lignified Cuttings of Juníperus Sabína L.

Borovkov Vadim Valentinovich[α] & Demchenko Gleb Aleksandrovich[σ]

ABSTRACT

In Russian nurseries, growth powders are widely used for rooting semi-lignified cuttings of coniferous crops. Due to the fact that the range of such powders is represented by preparations with only one concentration of the active substance (4 (indol-3-yl) butyric acid) - 5 g / l (0.5% IBA), a study was conducted on the possibility of diluting the preparations with talc and crushed charcoal using the Kornevin powder as an example. Semi-lignified cuttings of Juníperus sabína were used in the experiments; rooting was carried out under the conditions of installing low-pressure artificial fog with substrate heating. It was shown that the best option under the experimental conditions was the use of Kornevin-talc powder in a volume ratio of 1 to 1 to stimulate rooting. The rooting of the cuttings was 89.3%. Undiluted Kornevin had a phytotoxic effect, which caused a decrease in the survival rate from the values of the best option by 26%. The use of powders with a more significant dilution of Kornevin led to the appearance of signs of auxin deficiency in the stimulator. Thus, it was shown that for rooting cuttings of Juníperus sabína, powders with an IMC content of 0.25% are needed, which can be obtained by diluting Kornevin powder with talc or crushed charcoal. It was shown that when diluting growth powder, it is necessary to take into account that with the same degree of dilution (by powder volume), the hormonal properties of IMC decrease more intensively in options with crushed charcoal than talc.

Keywords: juníperus sabína, propagation, rooting, growth powders, auxins.

*Author*α: Nursery of ornamental plants "Vashutino" (141400, Moscow region, Khimki, Vashutinskoe shosse, Vashutino village, building 712, room 2), scientific consultant, agronomist.
σ: Nursery of ornamental plants "Vashutino" (141400, Moscow region, Khimki, Vashutinskoe shosse, Vashutino village, building 712, room 2), director of the nursery.

I. INTRODUCTION

Juníperus sabína L. is a creeping form of coniferous shrub, due to which it is an easily rooted coniferous crop. The survival rate of cuttings of many varieties without the use of rooting stimulants is 80-100% [1,2]. Despite this fact, nurseries use stimulation of root formation of this and other easily rooted species of coniferous crops in order to accelerate rhizogenesis and form a better root system, which reduces the time it takes to obtain rooted cuttings ready for transplantation [3,4,5]. There is also a justified need to use a stimulant when cuttings of such crops are prepared from aged - 10-15 year old mother plants [6].

At the same time, we must not forget that the unjustified use of rhizogenesis stimulants can lead to phytotoxicity up to the death of cuttings [7]. Such data were obtained during rooting of Picea A.Dietr. [8], Thuja occidentalis [9,10], Juníperus sabína L.and Juniperus communis L. [11], and Juniperus x pfitzeriana. In this regard, it is necessary to select the optimal concentration of the stimulant for a

London Journal of Research in Science: Natural & Formal

specific crop, rooting conditions, age of mother plantings, and other factors [12]. For example, when studying the range of IMC concentrations from 0 to 8 g/l in an alcohol solution when dipping the bases of Juníperus sabína L. cuttings for 5 seconds, the best concentration was 1 g/l IMC. Concentrations above 4 g/l IMC reduced rooting [13].

A method of stimulating the rooting of cuttings by dusting their bases with growth powder is widely used in Russian nurseries. With this method, there is no need to tie the cuttings into bundles, there is no need to subject the cuttings to additional soaking and storage, which can lead to infection with phytoparasitic organisms. This method is also widely used abroad and there is a whole range of growth powders with different concentrations of the active substance. For example, the line of powders produced by Rizopon (Netherlands) is represented by growth powders Chrysatop and Rizopon AA with an IMC content of 0.1%, 0.25%, 0.4%, 0.5%, 0.8%, 1%, 2%. On the Russian market, similar growth powders are represented by preparations containing only one concentration of the active substance - 5 g / kg IMC (0.5%, 4 (indol-3yl) butyric acid) [14]. In this regard, we conducted a study on the possibility of using Kornevin growth powder for rooting semi-lignified cuttings of Cossack juniper, including by diluting it to reduce the concentration of the active substance.

II. MATERIALS AND METHODS

The studies were conducted at the Vashutino production nursery of ornamental plants in a branch located in the city of Zubtsov, Tver Region. Semi-lignified cuttings of Cossack juniper (Juníperus sabína L.) were used in the studies. The cuttings were planted for rooting on April 30, 2022, in film gable cutting beds 0.6-0.9 m high, equipped with low-pressure fog and floor heating. The cutting beds were placed inside a film hangar greenhouse equipped with air heating and fine-droplet air cooling. Additionally, a shade made of white spunbond with a density of 60 g/m3 was installed under the roof of the greenhouse. The illumination range of the cuttings during the daytime was from 2000 to 15000 lux. The average switching mode of the fogging unit on sunny days was 5 seconds every 30 minutes; on cloudy days, the cuttings were sprayed once a day. Talc and charcoal crushed to a powder state were used to reduce the concentration of IMC in Kornevin. The ratio of the components during mixing was made by volume, since the density of crushed charcoal is two times lower than talc and Kornevin. According to the technological scheme, the cuttings were completely dipped in a solution of fundazole 5 g/10 liters, powdered with stimulants according to the manufacturer's recommendation and the adopted method [15]. The cuttings were planted in cassettes by sticking them into the substrate to a depth of 2-3 cm. The cuttings rooted without a stimulator served as a control. A mixture of slightly decomposed high-moor peat with a pH of 4.8-5.3 with preliminary application of Trichocin at a dose of 30 g/m3 and agroperlite of a fraction of 1-5 mm in a ratio of 2 parts peat to 1 part perlite 4-5 days before was used as a rooting substrate. The cassettes were placed in cutting boxes randomly among the production cassettes in seven replicates with 14 cuttings per replicate, a total of 784 cuttings. The experimental results were processed according to the dispersion analysis [16]. The cuttings were examined and the results of the study were calculated on the 188th day after planting the cuttings for rooting.

III. RESULTS OF THE STUDY AND THEIR DISCUSSION

The rooting of cuttings in the control variant was 10.7%, the average number of roots per cutting was the lowest of all variants - 1.36 pcs, a large number of cuttings formed callus - 44.59%, the maximum value of all variants (Figure 1, 2). We assume that the low value of cuttings survival in the control variant for such an easily rooted crop as Cossack juniper is explained by the significant age of the mother plants.

Figure 1: Semi-lignified cuttings of Juníperus sabína L., control variant (rooting without treatment in growth powders). The age of the mother plants is 8 years. Planting for rooting on 04/30/2022, calculation of results - 11/04/2022

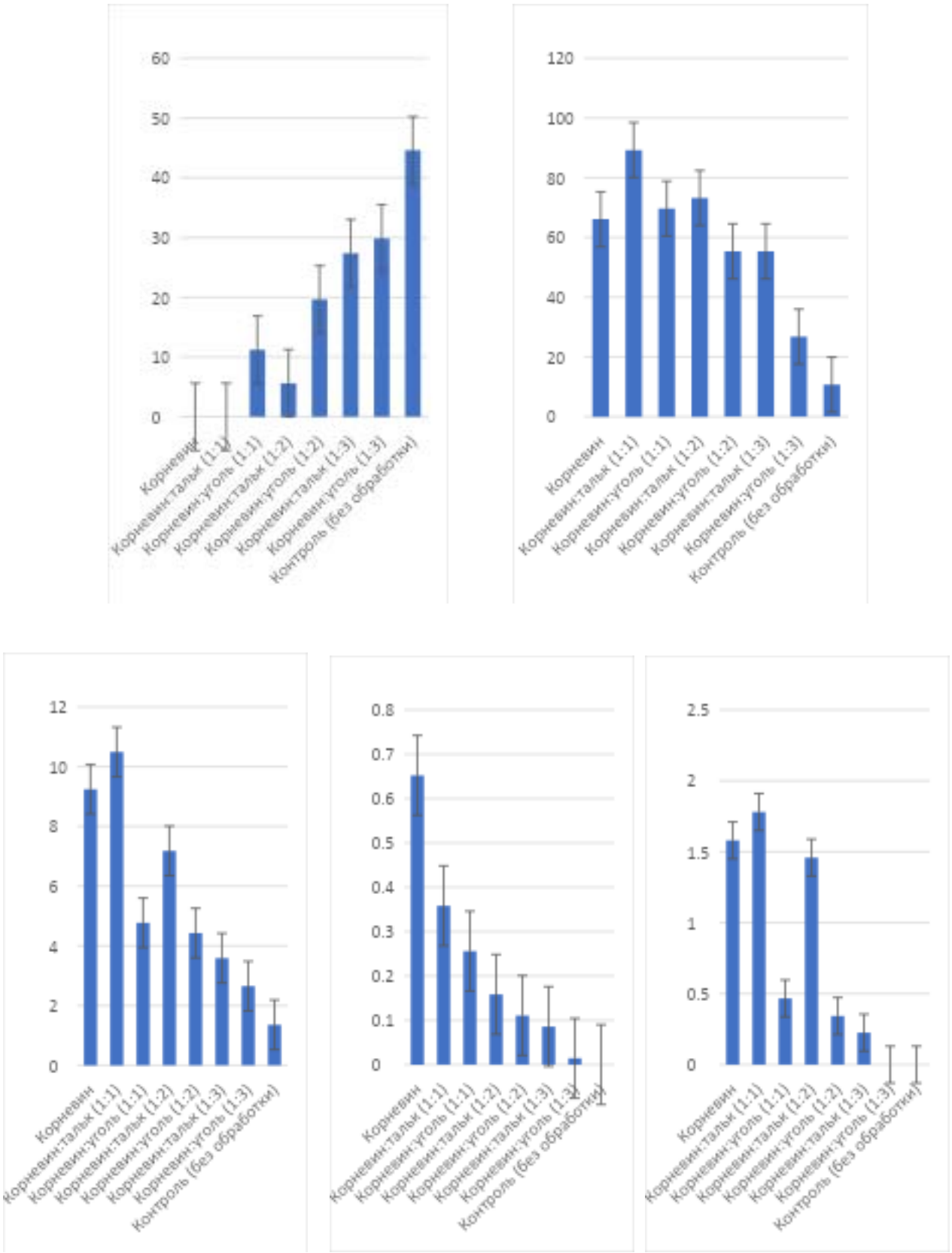

Figure 2: Changes in the rooting rates of semi-lignified cuttings of Juníperus sabína L. with a decrease in the IMC content in growth powders based on Kornevin. The age of mother plants is 8 years. Planting for rooting was on 30.04.2022, results were calculated on 04.11.2022.

The use of Kornevin (0.5% IMC) gave a significant positive effect on rooting. The survival rate of cuttings increased by 6.17 times to 66.1%, the average number of roots per cutting increased by 6.8 times and amounted to 9.2 pcs. (Figure 3). As expected, this variant showed phytotoxicity of the stimulator, which was characterized by the appearance of a "rotten base" in the cuttings [7], the average value of which was 0.65 cm. Diluting Kornevin with talc by two times (IMC content 0.25%) reduced phytotoxicity and increased the number of rooted cuttings by 23.2%, the average length of the "rotten base" decreased by 1.8 times and amounted to 0.36 cm. A statistically significant increase in the number of rooted cuttings after diluting Kornevin proves its phytotoxicity for the studied crop in its pure form. The obtained data show that 26% of the cuttings of the Kornevin:talc (1:1) variant could have died if undiluted Kornevin had been used.

Figure 3. Semi-lignified cuttings of Juníperus sabína L., Kornevin variant. The age of mother plants is 8 years. Planting for rooting was on 30.04.2022, results were calculated on 04.11.2022.

In the Kornevin:talc (1:2) variant, the IMC concentration was 0.17%, rooting decreased to 73.2%, the average number of roots decreased to 7.2 pcs., the average length of the rotten base and the length of the root zone decreased to 0.16 cm and 1.46 cm, respectively. The appearance of cuttings with callus (5.6%) in the Kornevin:talc (1:2) variant indicates a transition of the IMC concentration in the stimulator from excess to deficiency [5]. The presence of cuttings with callus (auxin deficiency) and a small proportion of cuttings with a "rotten base" (auxin excess) can be explained both by the different quality of cuttings with different endogenous auxin status, and by the error of the dusting method itself, when different amounts of powder fall on the cuttings.

Figure 4: Semi-lignified cuttings of Cossack juniper, Kornevin:talc (1:1) variant. Mother plants are 8 years old. Planting for rooting was carried out on 04/30/2022, resilts vere calculated on 11/04/2022.

The Kornevin:talc (1:3) variant containing 0.125% IMC showed a further decrease in rooting rates, and phytotoxicity ceased to be observed. Thus, the percentage of rooting of cuttings decreased by another 17.8% from the previous variant and amounted to 55.4%, the average number of roots decreased to 3.6 pcs. The average length of the root zone decreased by 6.6 times compared to the previous variant to 0.22 cm and began to tend to zero values of the control variant. The average length of the "rotten base" (a sign of phytotoxicity) decreased to zero values - to 0.09 cm, which is within the statistical error compared to the control variant. Callus formation, on the contrary, increased significantly - to 27.4%, which indicates an increase in the lack of auxin in the regulator. Thus, the best option in the series of studied powders Kornevin - Kornevin:talc was the option Kornevin:talc (1:1) with a rooting level of 89.3%.

For the dilution of Kornevin, charcoal ground into powder was also used. Since its density is two times less than that of Kornevin and talc, the dilution was done by volume. It is clear from the diagrams that when diluted with charcoal, the values of the rooting parameters change significantly towards a decrease in the concentration of IMC compared to the dilution of Kornevin with talc. Thus, the indicators of the Kornevin:charcoal (1:1) option are close in their values to the Kornevin:talc (1:2) option, and the indicators of the Kornevin:charcoal (1:2) option to the Kornevin:talc (1:3) option. A stronger decrease in the effect of the regulator at the same dilution in charcoal can occur due to the adsorption of part of the active substance and due to a change in the physical properties of the adhesion of the modified powder to the cutting. Conclusions.

When propagating the Cossack juniper, it is necessary to use growth powders with an IMC concentration of 2.5 g/kg (0.25%).

To obtain growth powders with a content of 0.25% IMC, it is necessary to modify Russian-made growth powders such as Kornevin (0.5% IMC) by diluting them with talc or crushed charcoal. When diluting the growth powder, it is necessary to take into account that with the same degree of dilution (by powder volume), the hormonal properties of IMC decrease more intensively in variants with crushed charcoal.
For specific rooting conditions, it is necessary to inspect the cuttings in order to identify signs of deficiency or phytotoxicity of the auxin concentration in the growth powder used for its correction using the proposed modification method.

REFERENCES.

1. Torchik, V. I. Rhizogenesis in ornamental garden forms of coniferous plants and methods of its intensification / V. I. Torchik, A. F. Kelko, G. A. Kholopuk. – Minsk: Republican Unitary Enterprise "Publishing House" Belarusian Science ", 2017. – 218 p.
2. Goncharenko, V. A. Vegetative propagation of ornamental forms of plants of the Cupressaceae family under conditions of an artificially intermittent fogging installation / V. A. Goncharenko, O. I. Korotkov, E. A. Shilovskaya // Plant biology and horticulture: theory, innovations. – 2020. – No. 1 (154). – P. 84-89.
3. Kiselevich, A. E. The influence of root formation stimulants and substrate heating on the rooting of green cuttings of western thuja (Thuja occidentalis) and Cossack juniper (Juniperus Sabina L) / A. E. Kiselevich // Current areas of scientific research in the 21st century: theory and practice. – 2013. – No. 4. – P. 108-113.
4. Matraimov, M. B. Propagation by stem cuttings of Juniperus sabina L. Using a growth stimulator (0.15 g Na + 0.9 g UA) / M. B. Matraimov // Science and new technologies. – 2011. – No. 5. – P. 110-113.
5. Borovkov, V. V. Callus formation as a physiological sign of auxin deficiency in the rhizogenesis stimulator (using the example of in vivo rooting of coniferous cuttings) / V. V. Borovkov, G. A. Demchenko // Bulletin of the Ufa Scientific Center of the Russian Academy of Sciences. – 2023. – No. 4. – P. 22-30
6. Ryabukhina M.V. Experience of cuttings of coniferous species in the conditions of Orenburg / M. V. Ryabukhina, S. S. Tyulebaeva, E. A. Samokhvalova, R. Z. Alibaev // Agrarian Bulletin of Primorye. – 2020. – No. 1(17). – P. 39-41.
7. Borovkov V.V. Physiological response to excessive doses of indole-3-butyric acid and its potassium salt in stimulating the rooting of semi-lignified cuttings of coniferous crops / V.V. Borovkov and G.A. Demchenko // BIO Web Conf., 139 (2024)
8. Dokuchaeva M.I. Vegetative propagation of conifers / Ed. by academician A.S. Yablokov. - Moscow: Lesnaya prom-st, 1967. - 105 p. ill.; 21
9. Pal'tseva, A. V. Propagation of representatives of the Cupressaceae family by green cuttings using rhizogenesis stimulants / A. V. Pal'tseva, A. N. Tseplyaev // Current issues of preserving biodiversity and sustainability of natural and artificial plant communities: Proceedings of the All-Russian youth scientific and practical conference, Voronezh, April 27, 2023 / Responsible. editor Yu.V. Chekmeneva. - Voronezh: Voronezh State Forest Engineering University named after G.F. Morozov, 2023. - P. 197-201.
10. Pinaeva, N. V. Experience of vegetative propagation of some species and varieties of conifers / N. V. Pinaeva, A. I. Dorokhova // Forestry and green construction in Western Siberia: Proceedings of the VII International Scientific Internet Conference, Tomsk, January 25, 2015. - Tomsk: TSU Publishing House, 2015. - P. 121-128. - EDN TRXQLD.

11. Rezvyakova, S. V. Reproduction of conifers by green cuttings using new biopreparations / S. V. Rezvyakova, A. G. Gurin, E. S. Rezvyakova // Bulletin of the Oryol State Agrarian University. - 2017. - No. 2 (65). - P. 9-14.
12. Borovkov, V. V. Stimulation of root formation in semi-lignified cuttings of Pfitzer juniper 'Pfitzeriana Glauca' (Juniperus × pfitzeriana 'Pfitzeriana Glauca') using growth powders with auxins / V. V. Borovkov, G. A. Demchenko // Forestry information. - 2023. - No. 3. - P. 94-102.
13. Abshahi M. Secondary metabolite changes in Maymars juniper cuttings (Juniperus sabina) under different treatments of propagation (IBA, substrate and harvest time of cutting) / M. Abshahi, H. Zarei, B. Zahedi, F.A. García¬Morote, A. Rezaei Nejad //Advances in Horticultural Science, 2022 36(3): 163¬-174
14. State Catalog of Pesticides and Agrochemicals as of December 2, 2024
15. Polikarpova F.Ya. Reproduction of Fruit and Berry Crops by Green Cuttings/F.Ya. Polikarpova//Agropromizdat – 1990 – 96 p.
16. Dospekhov B.A. Field Experiment Methodology / B.A. Dospekhov. Moscow: Kolos, 1973. - 336 p.